reaction mixture. Cy2-conjugated streptavidin was used to detect bound 82E1. Human brain sections (4-μm thickness) were obtained from paraffin-embedded tissue blocks. After deparaffinization and rehydration, endogenous peroxidase activity was quenched with 3% H_2O_2 (Sigma). Sections were subjected to heat-induced epitope retrieval followed by IgG blocking using M.O.M. kit (Vector Laboratories Inc., Burlingame, CA). Sections were incubated with RB4CD12 (1:100 dilution) overnight at 4°C. Bound antibody was detected with horseradish peroxidase-conjugated mouse anti-VSV followed by visualization with diaminobenzidine (3,3′-diaminobenzidinetetrahydrochloride) supplied with the EnVision reagent (Dako Japan, Tokyo, Japan).

Immunoelectron Microscopy

Cryostat-cut sections from 17-month-old Tg2576 mouse brains were prepared on MAS-coated glass slides, fixed in 4% paraformaldehyde for 5 minutes, and then washed with PBS for 1 hour. Sections were incubated with 3% bovine serum albumin for 30 minutes at RT. Diluted RB4CD12 antibody (1:40) was then applied overnight. After washing, diluted rabbit anti-VSV secondary antibody (7.2 μg/mL) was applied for 1 hour. After several washes, diluted goat anti-rabbit IgG antibody coupled with 1.4-nm-diameter tertiary gold particles (1:40) was applied for 30 minutes. The samples were then washed and fixed in 2% glutaraldehyde in 0.1 M sodium cacodylate buffer (pH 7.4) for 3 hours, followed by enlargement of the gold particles with an HQ-Silver Enhancement Kit (Nanoprobes). The specimens were examined in a Hitachi H-7600 transmission electron microscope (Hitachi Koki, Tokyo, Japan).

Immunoblots

The proteins (40 μg per lane) were separated by NuPAGE 3% to 8% polyacrylamide gel electrophoresis (Invitrogen, Carlsbad, CA), and blotted onto a polyvinylidene difluoride membrane (Millipore, Billerica, MA). The membrane was blocked with 5% skim milk/PBS 0.1% Tween for 1 hour at room temperature and then incubated overnight with RB4CD12 antibody (1:500) in TBS 0.1% Tween at 4°C. The membrane was washed and incubated with horseradish peroxidase-conjugated mouse anti-VSV (1:2000) for 1 hour at RT. Bound antibodies were visualized with SuperSignal West Dura Chemiluminescent reagent (Thermo Scientific). Signals were visualized and quantified using a LAS-3000 mini luminescent image analyzer (Fujifilm, Tokyo, Japan).

Preparation and Structural Analysis of HS

There were 100 mg of frozen brain tissues or the cortical vessel residue that remained on filters previously described, which was suspended in 2 mL of 0.2N NaOH and incubated overnight at RT. The samples were neutralized with 4 N HCl and then treated with DNase I and RNase A (0.04 mg/mL each) (Roche Diagnostics) in 50 mmol/L Tris-HCl, pH8.0, 10 mmol/L $MgCl_2$ for 3 hours at 37°C. Subsequently, the samples were treated with actinase E (0.08 mg/mL) (Kaken Pharmaceutical Co., Ltd., Tokyo, Japan) overnight at 37°C. The supernatant was collected by centrifugation at 5000 × *g* at 4°C for 10 minutes after heat inactivation of the enzyme and then mixed with the same volume of 50 mmol/L Tris-HCl, pH 7.2. The HS was purified by DEAE-Sepharose column chromatography.[9] The disaccharide compositions of the HS were determined by reversed-phase ion-pair chromatography with postcolumn fluorescent labeling.

Quantitative Real Time-PCR for Expression of Genes Related to HS Synthesis

Total RNA was extracted from frozen mouse cortices using TRIZol Reagent (Invitrogen). Total RNA (4 μg was used for reverse transcription reaction in 100 μL of buffer with random hexamers, using Superscript II Reverse Transcriptase (Invitrogen). PCR was conducted in duplicate with 20-μL reaction volumes of SYBR Premix Ex TaqII (Takara Bio Inc. Shiga, Japan), 0.2 μmol/L of each primer and 2 μL of the cDNA reaction mixture. PCR was performed using the following parameters: 95°C, 10 seconds, 1 cycle; 95°C, 5 seconds; and 60°C, 30 seconds, 40 cycles. Analysis was performed using sequence detection software supplied with Thermal Cycler Dice Real Time System TP800 (Takara Bio Inc.). mRNA levels of each gene were normalized by comparison to β-actin mRNA levels. Conclusions are drawn from duplicate PCR reactions at least two independent reverse transcription reactions. Primer sequences used in this study are as indicated for *Ndst1*, 5′-GCAGATGGCCCTGAACAA-GAA-3′ and 5′-GCACGTGCACAGGGTACACA-3′; for N-deacetylase/*N*-sulfotransferase 2 (*Ndst2*), 5′-TCATCCAG-AAGTTCCTGGGTATCAC-3′ and 5′-AGACAGCGAGTC-TTACCACCTTCAA-3′; for *Ndst3*, 5′-TCTGGTGTCAGCT-GCTGGAAG-3′ and 5′-CACGTTGTGGTCGCGGTAGTAG-3′; for *Ndst4*, 5′-TTGTTCCCAAAGCCAAGATCATTAC-3′ and 5′-TCAGGGCAGCTGGATCTTCA-3′; for *Hs6st1*, 5′-CT-GACTGGACCGAACTCACCAA-3′ and 5′-TCTCGCAGC-AGGGTGATGTAGTAG-3′; for *Hs6st2*, 5′-AAACTTCAACT-CAGGCGCCAAC-3′ and 5′-CTCCATTCACTCAAGTACCGT-GACA-3′; for *Hs6st3*, 5′-GACTGGACCGAGCTCACCAA-3′ and 5′-CATGCTTCCATTCGCTCAGGTA-3′; for *Hs2st1*, 5′-GCAAGCACCTCGTTCACCAA-3′ and 5′-CATCTCGTTC-CAGGTGGTTATGTTC-3′; for *Sulf1*, 5′-CCACATGGAGTT-CACCAACGTC-3′ and 5′-TAGCCGTGGTCCGCAGTGTA-3′; for *Sulf2*, 5′-GAGTACCAGACAGCATGCGAACA-3′ and 5′-TTGGGCACCAGGTTGGAGA-3′; and for *Actb*, 5′-CATCCG-TAAAGACCTCTATGCCAAC-3′ and 5′-ATGGAGCCAC-CGATCCACA-3′.

Statistical Analysis

All data are presented as means ± SD unless noted otherwise. The values were analyzed by unpaired Student's *t*-test using Prism software (GraphPad Software, La Jolla, CA). *P* values less than 0.05 were considered to be statistically significant.

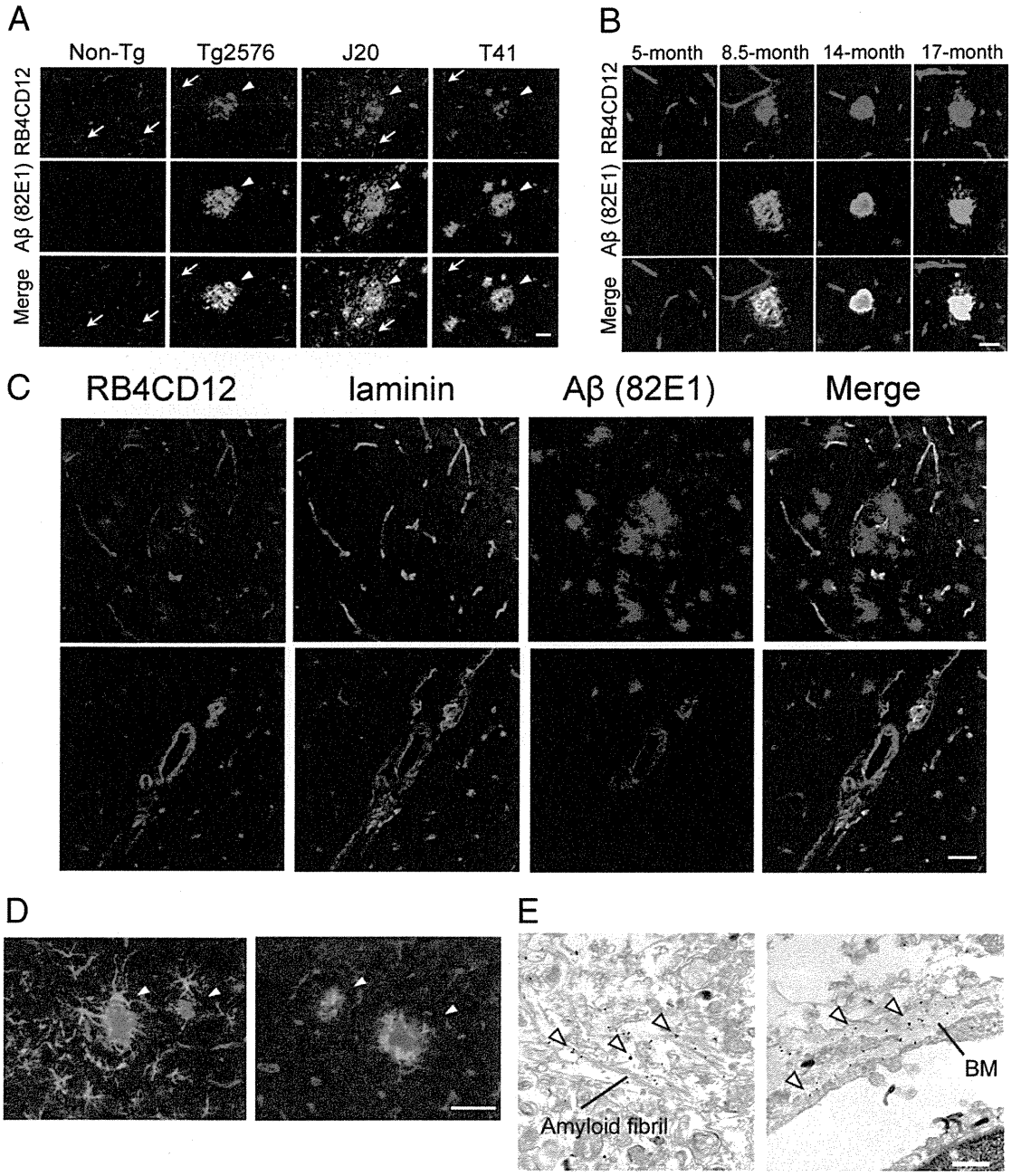

Figure 1. RB4CD12 anti-heparan sulfate epitope colocalizes with amyloid β plaques in the brain of Tg2576, J20, and T41 mice. **A:** Cryostat-cut brain sections of 18-month-old non-Tg and Tg2576, 23-month-old J20, and 12-month-old T41 mice were stained with RB4CD12 anti-HS antibody (red) and 82E1 anti-amyloid β (Aβ) antibody (green). Staining signals in vessels (**arrows**) and amyloid plaques (**arrowheads**) are shown. **B:** Expression of the RB4CD12 epitope and Aβ in aging Tg2576 brain. **C:** Expression of the RB4CD12 epitope, Aβ and laminin, a marker for vessels in the 18-month-old Tg2576 brain. **D:** Co-staining of RB4CD12 anti-HS antibody (red) with cell type-specific antibodies against glial fibrillary acidic protein astrocytes (**left**) or Iba1 microglia (**right**) (green). Co-stained areas are shown in yellow. **E:** Immunoelectron microscopy for the RB4CD12 epitope in amyloid fibrils in the brain of 18-month-old Tg2576 mouse. **Left panel** shows RB4CD12 signals in amyloid fibrils indicated by **arrowheads**. **Right panel** shows RB4CD12 signals in the basement membrane of vessels. BM, basement membrane. Scale bars (in **A**, **C**, and **D**): 50 μm. Scale bars (in **B** and **E**): 20 μm and 500 nm, respectively.

Results

Immunoreactivity of RB4CD12 Anti-Heparan Sulfate is Colocalized with Aβ Plaques in Brains of Transgenic Mouse Models of AD

RB4CD12 scFv antibody recognizes trisulfated disaccharide-containing highly sulfated domains within HS.[8,21] The RB4CD12 epitope has been shown to be present abundantly in the vasculature of the brain in mice.[9] We first analyzed expression of the RB4CD12 epitope in the brain of transgenic mouse models of AD. Tg2576 mice express mutated human amyloid precursor protein in the brain and show numerous Aβ plaques in the cortex and hippocampus.[18] The localization of the RB4CD12 highly sulfated domains in Aβ plaques was observed in an 18-month-old Tg2576 hippocampus (Figure 1A). The RB4CD12 epitope was immunolocalized in both diffuse

and neuritic amyloid plaques in the brain of Tg2576 (Figure 1, A–C). RB4CD12 also detected brain microvessels in Tg2576 mice. No specific staining was observed when RB4CD12 was substituted with MPB49, a non-HS scFv antibody (not shown). We also tested aged J20 and T41, other mouse models of AD. With respect to expression levels of Aβ peptides, Aβ42 is dominant in J20 and T41 mouse brains, whereas Aβ40 is dominant in Tg2576 mouse. We examined brain sections of these model mice immunohistochemically. The RB4CD12 highly sulfated domains were colocalized with Aβ plaques in the hippocampus of 23-month-old J20 and 12-month-old T41 mice (Figure 1A). To analyze age-dependent accumulation of the RB4CD12 epitope in Aβ plaques, we collected Tg2576 brains from 5-, 8.5-, 14- and 17-month-old mice. Aβ plaques were observed in 8.5-, 14- and 17-month-old Tg2576 brains. Cerebral Aβ deposition increases with age. RB4CD12 stained Aβ plaques at these ages (Figure 1B). Next, we investigated vasculature and non-vasculature RB4CD12 epitopes in aged Tg2576 brain by co-staining with antibodies against Aβ and laminin, a marker of vascular basement membranes. Immunoreactivity of RB4CD12 in vascular structure was colocalized with anti-laminin staining signals (Figure 1C). RB4CD12 staining signals that were not associated with signals of anti-laminin antibody predominantly colocalized with anti-Aβ staining signals in the cortex of Tg2576 mice (Figure 1C, upper panels). The RB4CD12 epitope was also observed in the vessel walls of Aβ-positive leptomeningeal vessels (Figure 1C, lower panels). Staining patterns of RB4CD12 were different from the immunoreactivity of glial fibrillary acidic protein, an astrocyte marker, and Iba-1, a microglia marker (Figure 1D). Immunoelectron microscopy confirmed the localization of RB4CD12 epitope within amyloid fibrils and the basement membrane (Figure 1E). The RB4CD12 immunoreactive area that is not colocalized with anti-laminin staining signals was determined by fluorescence microscopy and quantified with computer-aided image analysis. In Tg2576 cortex and hippocampus, RB4CD12-positive but laminin-negative area was increased to fourfold to fivefold of that in non-Tg (Figure 2). In contrast, no change was observed in the cerebellum where no Aβ plaques were observed (Figure 2). We noted that laminin-positive vessels had attenuated diameters and a more ragged profile in Tg2576 cortex and hippocampus (Figure 2).

The RB4CD12 Epitope Is Immunolocalized in Amyloid Plaques in Postmortem Brains of Alzheimer's Disease Patients

We tested RB4CD12 antibody for staining of brains from NDC individuals and AD patients (Table 1). In NDCs, vessel-staining signals were predominantly observed (Figure 3A). In AD entorhinal cortex, amyloid deposits, as well as vessels, were positive for RB4CD12 (Figure 3B). Amyloid deposits and microvessels were also stained with RB4CD12 in AD hippocampus (Figure 3C). Interestingly, some pyramidal neurons in AD hippocampus showed intracellular granular staining (Figure 3D). These intracellular staining signals were detected in a certain number of cells that were positive for hyperphosphorylated microtubule-associated protein tau as revealed by the AT180 monoclonal antibody (see Supplemental Figure S1 at *http://ajp.amjpathol.org*).

Expression of the RB4CD12 Epitope Borne in Molecules with 70–180 kDa Molecular Weights Is Upregulated in the Cortex of Tg2576 Mice

As an extension of the staining results in the mouse and human brain tissues, we wished to determine which proteins contain the RB4CD12 epitope and were differentially expressed in Tg2576 brains. We performed Western blotting for cortex samples, which were fractionated as TBS-insoluble/1% SDS-soluble. Four non-Tg and five Tg2576 mice (20 months old) were examined. Multiple bands were positive for RB4CD12 antibody in both non-Tg and Tg2576 (Figure 4A). We measured intensities of 460 kDa, 180 kDa, 120 kDa, and 100–70 kDa bands by densitometry. There was a 1.3-fold increase in the intensity of overall RB4CD12 recognition determinants in Tg2576 brain extracts compared with non-Tg controls (Figure 4B). Expression levels of RB4CD12 epitopes in bands of 180 kDa, 120 kDa, and 100–70 kDa were increased 1.1- to 1.5-fold in the cortex of Tg2576 mice (Figure 4B). There was no significant change in the intensity of bands of 460 kDa. Syndecan-3 and glypican-1 are HSPGs expressed in glial cells surrounding Aβ plaques of Tg2576 mice.[22] To ascertain whether these proteins are HSPGs that contain the RB4CD12 epitope, we then analyzed their expression. Western blotting revealed the protein bands at 250 to 180 kDa for syndecan-3 and 60 kDa for glypican-1 in the cortex of Tg2576 mice (see Supplemental Figure S2A at *http://ajp.amjpathol.org*). Expression levels of these proteins in the Tg2576 cortex were comparable to those in non-Tg controls (see Supplemental Figure S2B at *http://ajp.amjpathol.org*).

Disaccharide Compositions of HS and Expression Profiles of HS Enzymes in the Cortex of Tg2576 and Postmortem AD

We performed structural analysis of HS chains extracted from mouse and human postmortem brains (Table 1). HS was isolated from the cortex of mice or postmortem human entorhinal cortex. HS was depolymerized into its constituent disaccharides by a mix of bacterial heparitinases. The disaccharide compositions of the HS were determined by reversed-phase ion-pair chromatography. We found that the total HS contents and HS disaccharide compositions in vessel-enriched fractions ("vessel-enriched fr") and non-vessel associated fractions ("non-vasculature fr") were comparable between non-Tg and Tg2576 mice (Figure 4C). In human, the reduction in the proportion of non-sulfated disaccharides reached statistical significance. Total HS contents and percentages of other sulfated disaccharides were comparable between NDC and AD (Figure 4D). To understand possible mechanisms of upregulation of the RB4CD12 epitope in AD mouse brains, we measured mRNA levels of 10 HS modification enzymes by quantitative real time-PCR. HS enzymes include sulfotransferases and extracellular sulfatases. These enzymes are regarded as

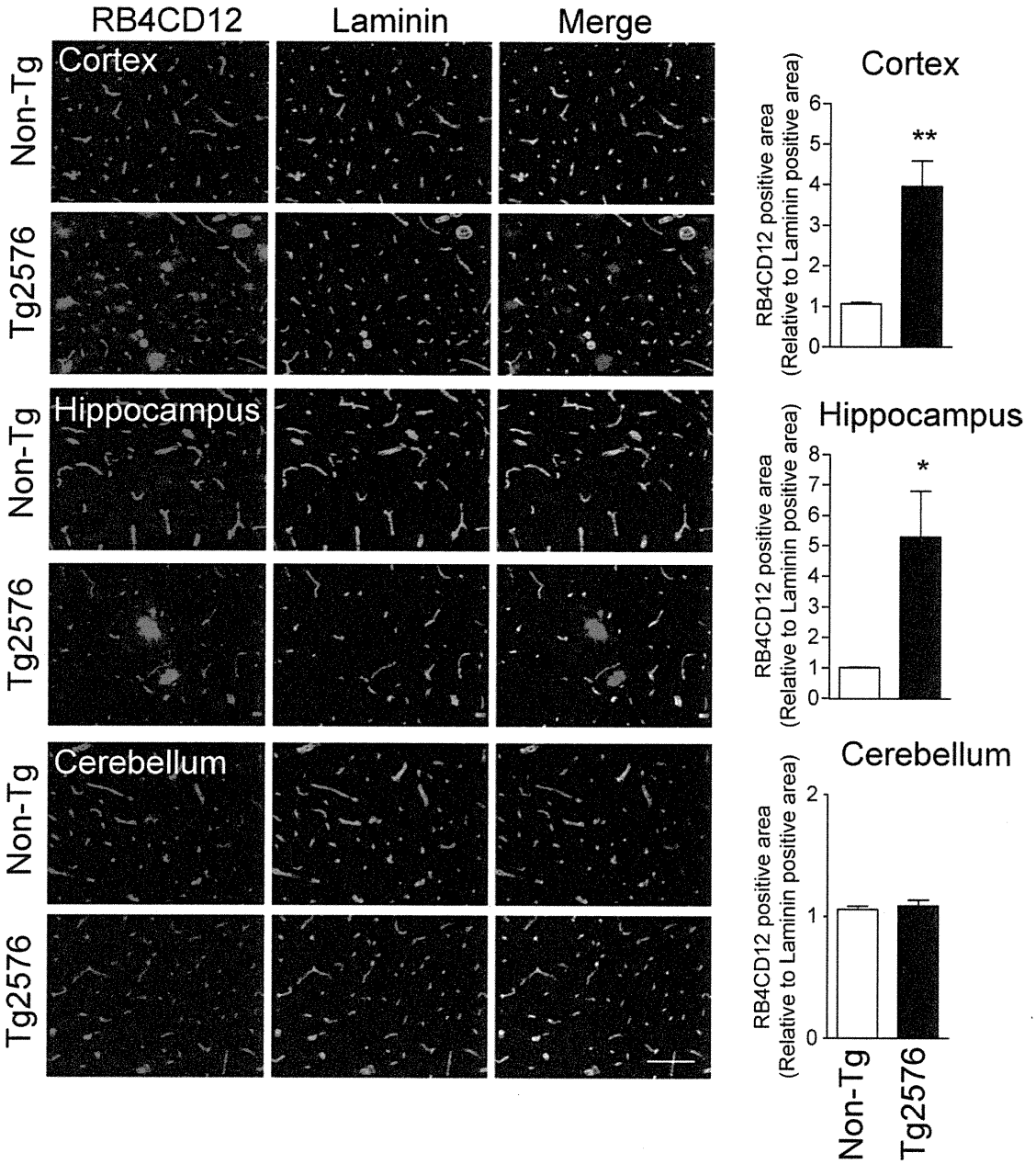

Figure 2. Quantification of the RB4CD12 epitope in nonvascular parenchyma in the brain of Tg2576 mice. Cryostat-cut brain sections of Tg2576 mice were stained with RB4CD12 (red) and anti-laminin (green) antibodies. Laminin is a marker for brain vessels. Nonvascular amyloid β plaques were stained with RB4CD12 antibody in the cortex and hippocampus. Graphs are of semiquantitative analysis of immunohistochemical pictures of RB4CD12 and laminin. RB4CD12-positive areas that were not colocalized with anti-laminin staining signals were calculated. $^{*}P < 0.05$, $^{**}P < 0.01$.

key molecules in the regulation of sulfation of HS. The mRNA level of N-deacetylase/N-sulfotransferase 2 were significantly increased in Tg2576 (24%) (Figure 4E). The mRNA levels of Sulf-1 and Sulf-2 were comparable between non-Tg and Tg2576 mice (Figure 4E).

Sulf-1 and Sulf-2, Extracellular HS Sulfatases, Degrade the RB4CD12 Epitope Accumulated in Amyloid Plaques

Previously, we showed that the treatment of wild-type mouse brain sections with Sulf-1 or Sulf-2 greatly diminished the RB4CD12 epitope abundant in vasculature.[8] To determine whether the RB4CD12 epitope in amyloid plaques is susceptible to Sulf-1 and Sulf-2 and degraded by these enzymes, we treated cryo-cut brain sections of 18-month-old Tg2576 mice with recombinant Sulf-1, Sulf-2, or conditioned medium of MCF-7 breast cancer cells, which secrete native Sulf-2.[23] These treatments substantially reduced the RB4CD12 epitope in sections of Tg2576 brain *ex vivo* (Figure 5). A mixture of bacterial heparinases confirmed that the assay is suitable for *ex vivo* degradation of HS in brain sections and that the observed signals arose from HS (Figure 5). Anti-Aβ staining signals that were colocalized with the RB4CD12 epitope were retained after Sulf treatment (Figure 5).

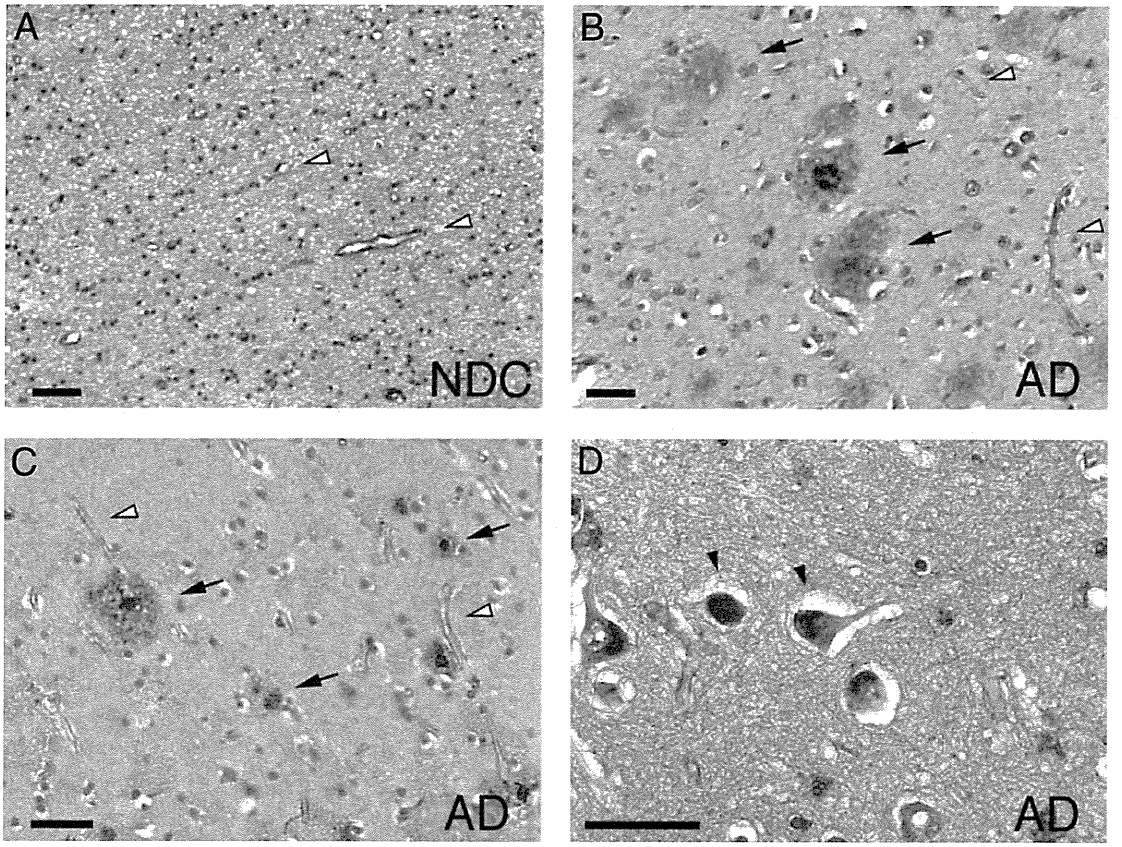

Figure 3. RB4CD12 epitope immunolocalizes in amyloid plaques in the brains of Alzheimer's disease patients. Immunoperoxidase staining for RB4CD12 (brown) in the entorhinal cortex (**A**, **B**) and hippocampus (**C**, **D**). **Open arrowheads** in **A–C** show vessel-staining signals in brains of non-demented control (NDC) and Alzheimer's disease (AD). In AD, amyloid deposits were also positive for RB4CD12 (**arrows** in **B** and **C**). Intracellular RB4CD12-staining signals are seen in some hippocampal neurons of AD (**arrowheads** in **D**). Scale bars: 50 μm.

Discussion

In the present study, we showed that the RB4CD12 epitope is colocalized with amyloid plaques in brains of AD mouse models and patients with AD. Consistent with our previous report,[9] the RB4CD12 epitope was also colocalized with laminin-positive vasculature in brains of mouse models of AD. Quantification analysis revealed that the non-vascular RB4CD12-positive area was increased in the cortex and hippocampus of Tg2576, J20, and T41 AD models. In the cerebellum, where no amyloid plaques were observed in these model mice, RB4CD12 staining was comparable to that in the non-Tg. Morphological alterations of the vasculature observed in the cortex and hippocampus of Tg2576 were consistent with the previous report that Aβ aggregates induce the structural and functional disruption of smooth muscle cells in the vasculature.[24] Results in aging brains of Tg2576 mice suggested that Aβ and the HS highly sulfated domains start accumulation at the same age. Aβ and other self-aggregating peptides share cationic motifs that may be involved in binding to the negative charges of sulfated glycosaminoglycan.[25,26] HS and other glycosaminoglycan chains can stabilize mature fibrils against proteolytic degradation.[27] HS facilitates the formation of fibrils of amylin,[17] apo-serum amyloid A,[28] α-synuclein,[29] prion protein,[30] muscle acylphosphatase,[31] transthyretin,[32] Tau,[33] and Aβ.[34–36] *In vivo* fragmentation of heparan sulfate by heparanase overexpression could protect mice from amyloid protein A amyloidosis.[37] Importantly, the degree of sulfation is critical for enhancement of fibrillogenesis of Aβ.[35] Pathological effects of heparin in Aβ aggregation assays are dependent on sulfate moieties at N- and O-positions.[38] Our findings of selective accumulation of the RB4CD12 epitope in amyloid plaques suggest that highly sulfated domains of HS could play an important role in the progression of Aβ deposition. HSPG facilitates cerebral amyloid deposition, which can be induced exogenously in a rat model.[15] Highly sulfated HS chains could be one candidate for heat-resistant materials present in the brain extract that are essential for exogenous induction of cerebral β-amyloidogenesis in mouse models.[39] Recently, Timmer et al[40] demonstrated that only a minimal number of Aβ plaques (~30%) were co-stained with the epitope of JM403, an anti-HS antibody, in aging brains of APPswe/PS1dE9 model mice. JM403 detects HS subdomains containing the positively charged disaccharide [-glucuronic/iduronic acid-N-unsubstituted glucosamine].[41] Future studies may reveal differential contribution of HS subdomains composed of specific disaccharide structures to AD pathogenesis. Possible involvement of the RB4CD12 epitope existing in laminin-positive vasculature in AD pathogenesis should also be clarified in the future. Interestingly, intraneuronal RB4CD12 staining was observed in the

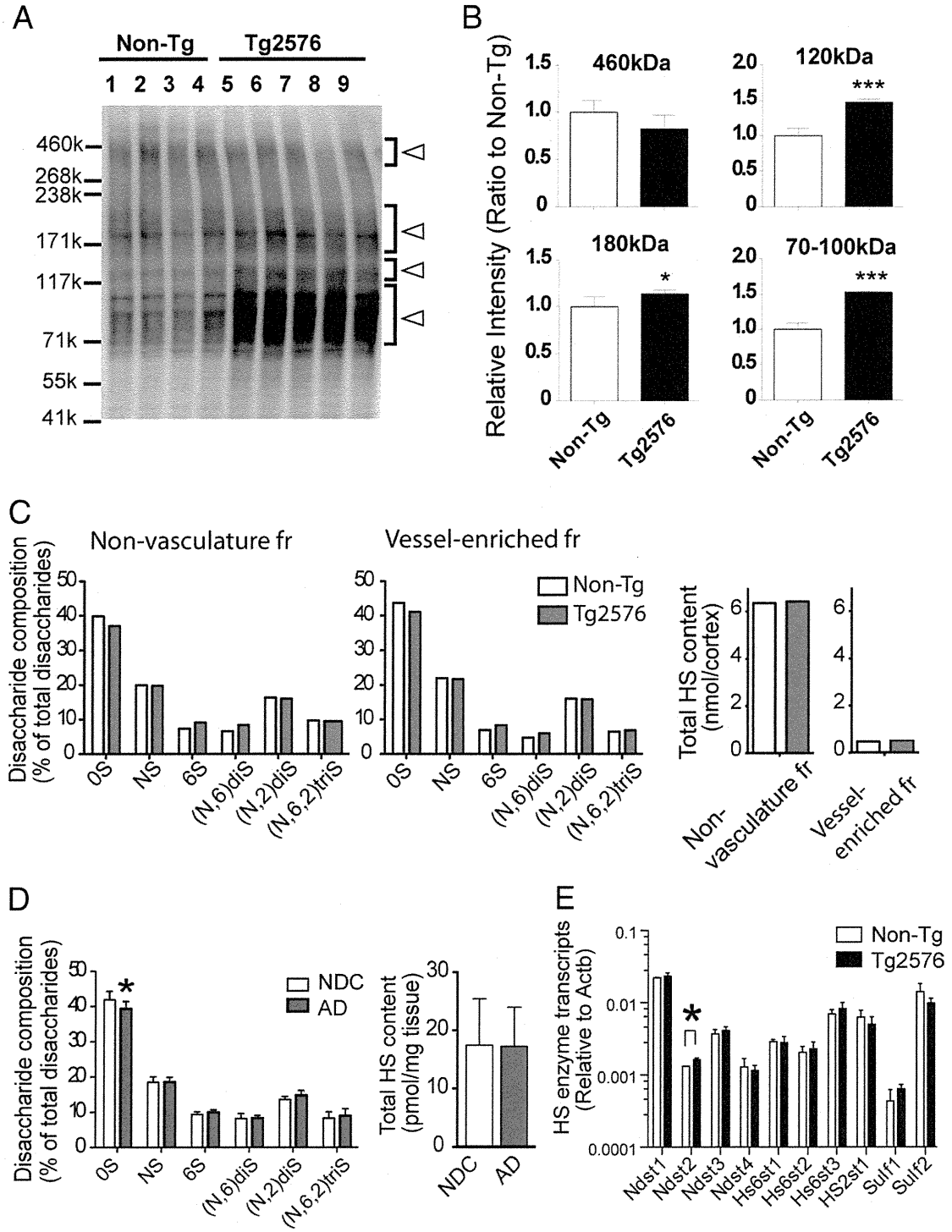

Figure 4. Immunoblotting analysis of the RB4CD12 epitope, disaccharide composition analysis of Heparan sulfate (HS) and quantitative real-time PCR analysis of HS enzymes in the brain of Tg2576 mice. **A:** Tris-buffered saline (TBS)-insoluble/1% SDS-soluble fractions were prepared from tissue homogenates of four 20-month-old Tg2576 (lanes 1–4) and five 20-month-old non-Tg (lanes 5–9) cortices. Immunoblot with RB4CD12 was performed as described in *Materials and Methods*. **B:** Relative intensities of bands with molecular weights of 460 kDa, 180 kDa, 120 kDa, and 70 to 100 kDa indicated by **open arrowheads** in (**A**) were measured. **C:** High performance liquid chromatography analysis determined non-sulfated (0S), monosulfated (NS, 6S), disulfated ([N,6]diS, [N,2]diS) and trisulfated ([N,6,2]triS) disaccharide compositions in non-vasculature fractions and vessel-enriched fractions of 18-month-old non-Tg and Tg2576 cortices. The level of total HS was determined by summing amounts of all disaccharides detected in each fraction. The values are representative of two independent experiments. **D:** HS disaccharide compositions and the level of total HS in the entorhinal cortex of non-demented control (NDC) ($n = 8$) and Alzheimer's disease (AD) ($n = 8$) postmortem brains were determined. **E:** Total-RNA from the cerebral cortices of 18-month-old Non-Tg ($n = 3$) and Tg2576 mice ($n = 3$) were prepared and tested. mRNA levels of 10 HS modification enzymes were determined by quantitative real-time PCR. $^{*}P < 0.05$, $^{***}P < 0.001$.

hippocampus of AD patients. Microtubule-associated protein Tau is the major protein subunit of intraneuronal neurofibrillary tangles, another neuropathological hallmark of AD.[42] It has been shown that Tau and HS coexist in nerve cells with overt neurofibrillary lesion.[33] The filamentous structures induced by heparin are structurally similar to those found in Alzheimer's disease.[43–45] We have shown that some of RB4CD12

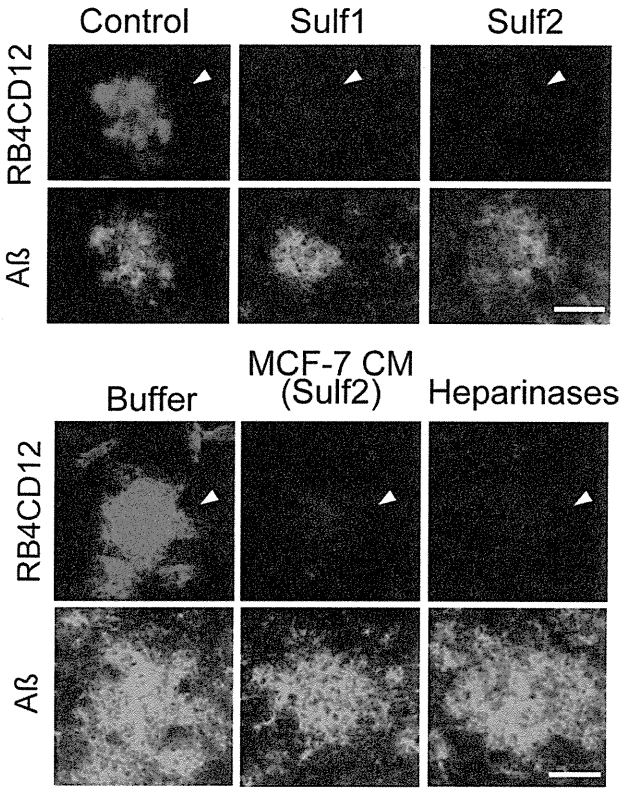

Figure 5. The RB4CD12 epitope in amyloid plaques of Tg2576 mouse brains is degraded *ex vivo* by Sulf-1, Sulf-2 and conditioned medium of Sulf-2-expressing cells. Cryostat-cut consecutive sections of 18-month-old Tg2576 mouse brains were incubated overnight with recombinant human Sulf-1 and Sulf-2 prepared from CM of transfected HEK293 cells (Sulf1, Sulf2), buffer only (Buffer), or CM of MCF-7 human breast cancer cells (MCF-7 CM).[8,23] The Ni-NTA resin-bound materials that were prepared from HEK293 cells transfected with the empty vector were eluted and used (control). A mix of bacterial heparinases (heparinases) served as a positive control. RB4CD12 binding was visualized using a Cy3-conjugated anti-VSV tag antibody (red). Treated sections were co-stained with 82E1 anti-Aβ antibody (green). The data are representative of two independent experiments. **Arrowheads** indicate amyloid plaques. Scale bars: 20 μm.

staining signals were found in cells that were stained with AT180, an antibody against hyperphosphorylated tau. Our results suggest that highly sulfated domains of HS might play a role in the formation of neurofibrillary tangles.

In immunoblots of brain lysates with the RB4CD12 antibody, we detected several RB4CD12-positive bands in non-Tg and Tg2576 mouse brains and found that 180 kDa, 120 kDa, and 100–70 kDa bands were upregulated in the cortex of Tg2576 mice. There were no significant changes in the intensities of 460 kDa bands. Our previous results showed that the RB4CD12 epitope is abundant in the basement membrane of the brain vessels and that the RB4CD12-positive bands were predominantly 460 kDa bands in brain vessel fractions.[9] In our immunohistochemical studies, non-vascular RB4CD12 staining was increased in Tg2576 mice. These results suggest that upregulation of 180 kDa, 120 kDa, and 100–70 kDa bands could contribute to the RB4CD12 staining colocalized with amyloid plaques in Tg2576 mouse brain. Several HSPGs are known to be localized in amyloid plaques.[14,46–49] Because of the high molecular weight (>210 kDa) of agrin and perlecan, it is conceivable that the observed signals in immunoblots might have arisen from other molecules. Syndecan-3 and glypican-1 in glial cells were identified as molecules associated with Aβ deposits.[22] Our Western blotting results suggested that syndecan-3 with the molecular weights of 180 to 250 kDa could be an HSPG that possesses the RB4CD12 epitope. However, we cannot rule out the possibility that degradation products of agrin or perlecan could harbor the RB4CD12 epitope observed in amyloid plaques. We should also pay attention to possible accumulation of HS degradation products catalyzed by nitric oxide.[50]

Unexpectedly, the trisulfated disaccharide composition was not increased in either Tg2576 or human postmortem AD brains. The mechanisms underlying the accumulation of the RB4CD12 highly sulfated domains within HS polysaccharides in non-vasculature amyloid plaques are not clear. There are two possibilities to explain the mechanisms. First, the N-sulfation of glucosamine residues is the initial HS sulfation and the N-sulfated domains are primary sites for further modification.[51] Consecutive occurrence of N-sulfation could be attributable to the formation of trisulfated disaccharide clusters, namely, highly sulfated domains, within HS chains in non-vasculature spaces. Second, translocation of HS that contains the RB4CD12 highly sulfated domains between brain vasculature and non-vasculature could be an explanation for the accumulation of the RB4CD12 epitope in Tg2576 brain parenchyma. Our findings that comparable levels of disaccharide compositions and HS contents in vessel-enriched fractions and non-vasculature fractions in the cortex of Tg2576 were shown and that the mRNA level of N-deacetylase/N-sulfotransferase 2 was increased in the cortex of Tg2576 mouse could support the former possibility. A previous study by Lindahl et al[52] showed altered distribution of N-sulfated glucosamine residues within HS extracted from postmortem AD brain. Highly N-sulfated HS may be involved in the initiation of the aggregation process of Aβ in AD brains.[53] These studies also support the former possibility as an explanation of the mechanisms of accumulation of RB4CD12-positive highly sulfated domains in Aβ plaques. We cannot rule out the possibility that the RB4CD12 epitope is a minor component and that the structural analysis we have performed might not fully detect the minor change. Quantitative analysis for the RB4CD12-positive HS in the cortex would make advances in the study of the mechanisms.

Herein, we found that the RB4CD12 epitope accumulated in amyloid plaques can be degraded by Sulf-1 and Sulf-2 *ex vivo*. It was suggested that the RB4CD12 highly sulfated domains are localized at the surface of amyloid plaques, as these HS degrading enzymes could access and efficiently degrade the epitope. Although the RB4CD12 epitope in amyloid plaques was degraded by the Sulfs, substantial amounts of Aβ were retained in these plaques. This result suggests that the highly sulfated domains of HS universally associated with amyloid deposits in the brain. Accumulation of the RB4CD12 epitope in amyloid plaques could induce excessive entrapment of growth factors at amyloid plaques, which might lead to an imbalance in homeostasis of the brain microenvironment. Increasing evidence points to vascular damage as an early contributor in Alzheimer pathology.[54,55] A recent study suggested that angiogenesis

might be impaired in AD model mice,[56] despite the fact that the levels of pro-angiogenic growth factors (eg, vascular endothelial growth factor [VEGF]) are elevated in AD brains.[57–59] VEGF binds to immobilized heparin and can be stored in the extracellular space by binding to HS and HSPG.[23,60] Heparin-bound VEGF is mobilized by the action of Sulf-2, which exerts pro-angiogenic activity.[23,61] VEGF is found to be associated with amyloid plaques in AD, but not non-AD brain.[62] Our results also suggested that the highly sulfated domains could be involved in sequestration of VEGF within amyloid plaques and vascular damage in AD through perturbation in the supply of pro-angiogenic growth factors. Aberrant angiogenesis could induce neurovascular uncoupling, which ultimately leads to synaptic dysfunction.[63] In summary, we provide evidence that highly sulfated domains recognized by RB4CD12 accumulated in amyloid plaques of brains of AD model mice and patients with AD. Further studies to investigate the roles of the highly sulfated HS domains with special regard to angiogenesis in AD pathology will be needed.

Acknowledgments

We thank Steven Rosen and Yoshiko Takeda-Uchimura for their helpful suggestions and discussions. We also thank Kuniko Takanose, Noriko Sugaya, and Hudson Johns for their technical assistance. We are grateful to Yoshio Hashizume and Takayuki Yamamoto for their diagnostic examination and support.

References

1. Bernfield M, Gotte M, Park PW, Reizes O, Fitzgerald ML, Lincecum J, Zako M: Functions of cell surface heparan sulfate proteoglycans. Annu Rev Biochem 1999, 68:729–777
2. Esko JD, Lindahl U: Molecular diversity of heparan sulfate. J Clin Invest 2001, 108:169–173
3. Gallagher JT: Heparan sulfate: growth control with a restricted sequence menu. J Clin Invest 2001, 108:357–361
4. Nakato H, Kimata K: Heparan sulfate fine structure and specificity of proteoglycan functions. Biochim Biophys Acta 2002, 1573:312–318
5. Parish CR: The role of heparan sulphate in inflammation. Nat Rev Immunol 2006, 6:633–643
6. Bishop JR, Schuksz M, Esko JD: Heparan sulphate proteoglycans fine-tune mammalian physiology. Nature 2007, 446:1030–1037
7. Dennissen MA, Jenniskens GJ, Pieffers M, Versteeg EM, Petitou M, Veerkamp JH, van Kuppevelt TH: Large, tissue-regulated domain diversity of heparan sulfates demonstrated by phage display antibodies. J Biol Chem 2002, 277:10982–10986
8. Hossain MM, Hosono-Fukao T, Tang R, Sugaya N, van Kuppevelt TH, Jenniskens GJ, Kimata K, Rosen SD, Uchimura K: Direct detection of HSulf-1 and HSulf-2 activities on extracellular heparan sulfate and their inhibition by PI-88. Glycobiology 2010, 20:175–186
9. Hosono-Fukao T, Ohtake-Niimi S, Nishitsuji K, Hossain MM, van Kuppevelt TH, Michikawa M, Uchimura K: RB4CD12 epitope expression and heparan sulfate disaccharide composition in brain vasculature. J Neurosci Res 2011, 89:1840–1848
10. Esko JD, Selleck SB: Order out of chaos: assembly of ligand binding sites in heparan sulfate. Annu Rev Biochem 2002, 71:435–471
11. Saad OM, Ebel H, Uchimura K, Rosen SD, Bertozzi CR, Leary JA: Compositional profiling of heparin/heparan sulfate using mass spectrometry: assay for specificity of a novel extracellular human endosulfatase. Glycobiology 2005, 15:818–826
12. Morimoto-Tomita M, Uchimura K, Werb Z, Hemmerich S, Rosen SD: Cloning and characterization of two extracellular heparin-degrading endosulfatases in mice and humans. J Biol Chem 2002, 277:49175–49185
13. Snow AD, Mar H, Nochlin D, Kimata K, Kato M, Suzuki S, Hassell J, Wight TN: The presence of heparan sulfate proteoglycans in the neuritic plaques and congophilic angiopathy in Alzheimer's disease. Am J Pathol 1988, 133:456–463
14. Snow AD, Sekiguchi RT, Nochlin D, Kalaria RN, Kimata K: Heparan sulfate proteoglycan in diffuse plaques of hippocampus but not of cerebellum in Alzheimer's disease brain. Am J Pathol 1994, 144: 337–347
15. Snow AD, Sekiguchi R, Nochlin D, Fraser P, Kimata K, Mizutani A, Arai M, Schreier WA, Morgan DG: An important role of heparan sulfate proteoglycan (Perlecan) in a model system for the deposition and persistence of fibrillar A beta-amyloid in rat brain. Neuron 1994, 12:219–234
16. van Horssen J, Wesseling P, van den Heuvel LP, de Waal RM, Verbeek MM: Heparan sulphate proteoglycans in Alzheimer's disease and amyloid-related disorders. Lancet Neurol 2003, 2:482–492
17. Watson DJ, Lander AD, Selkoe DJ: Heparin-binding properties of the amyloidogenic peptides Abeta and amylin. Dependence on aggregation state and inhibition by Congo red. J Biol Chem 1997, 272: 31617–31624
18. Hsiao K, Chapman P, Nilsen S, Eckman C, Harigaya Y, Younkin S, Yang F, Cole G: Correlative memory deficits. A beta elevation, and amyloid plaques in transgenic mice, Science 1996, 274:99–102
19. Mucke L, Masliah E, Yu GQ, Mallory M, Rockenstein EM, Tatsuno G, Hu K, Kholodenko D, Johnson-Wood K, McConlogue L: High-level neuronal expression of abeta 1–42 in wild-type human amyloid protein precursor transgenic mice: synaptotoxicity without plaque formation. J Neurosci 2000, 20:4050–4058
20. Rockenstein E, Mallory M, Mante M, Sisk A, Masliaha E: Early formation of mature amyloid-beta protein deposits in a mutant APP transgenic model depends on levels of A beta(1–42). J Neurosci Res 2001, 66:573–582
21. Jenniskens GJ, Oosterhof A, Brandwijk R, Veerkamp JH, van Kuppevelt TH: Heparan sulfate heterogeneity in skeletal muscle basal lamina: demonstration by phage display-derived antibodies. J Neurosci 2000, 20:4099–4111
22. O'Callaghan P, Sandwall E, Li JP, Yu H, Ravid R, Guan ZZ, van Kuppevelt TH, Nilsson LN, Ingelsson M, Hyman BT, Kalimo H, Lindahl U, Lannfelt L, Zhang X: Heparan sulfate accumulation with Abeta deposits in Alzheimer's disease and Tg2576 mice is contributed by glial cells. Brain Pathol 2008, 18:548–561
23. Uchimura K, Morimoto-Tomita M, Bistrup A, Li J, Lyon M, Gallagher J, Werb Z, Rosen SD: HSulf-2, an extracellular endoglucosamine-6-sulfatase, selectively mobilizes heparin-bound growth factors and chemokines: effects on VEGF. FGF-1, and SDF-1, BMC Biochem 2006, 7:2
24. Christie R, Yamada M, Moskowitz M, Hyman B: Structural and functional disruption of vascular smooth muscle cells in a transgenic mouse model of amyloid angiopathy. Am J Pathol 2001, 158:1065–1071
25. Diaz-Nido J, Wandosell F, Avila J: Glycosaminoglycans and beta-amyloid, prion and tau peptides in neurodegenerative diseases. Peptides 2002, 23:1323–1332
26. McLaurin J, Fraser PE: Effect of amino-acid substitutions on Alzheimer's amyloid-beta peptide-glycosaminoglycan interactions. Eur J Biochem 2000, 267:6353–6361
27. Gupta-Bansal R, Frederickson RC, Brunden KR: Proteoglycan-mediated inhibition of A beta proteolysis. A potential cause of senile plaque accumulation, J Biol Chem 1995, 270:18666–18671
28. Ancsin JB, Kisilevsky R: The heparin/heparan sulfate-binding site on apo-serum amyloid A. Implications for the therapeutic intervention of amyloidosis, J Biol Chem 1999, 274:7172–7181
29. Cohlberg JA, Li J, Uversky VN, Fink AL: Heparin and other glycosaminoglycans stimulate the formation of amyloid fibrils from alpha-synuclein in vitro. Biochemistry 2002, 41:1502–1511
30. Supattapone S: Prion protein conversion in vitro. J Mol Med 2004, 82:348–356
31. Motamedi-Shad N, Monsellier E, Torrassa S, Relini A, Chiti F: Kinetic analysis of amyloid formation in the presence of heparan sulfate: faster unfolding and change of pathway. J Biol Chem 2009, 284: 29921–29934

32. Noborn F, O'Callaghan P, Hermansson E, Zhang X, Ancsin JB, Damas AM, Dacklin I, Presto J, Johansson J, Saraiva MJ, Lundgren E, Kisilevsky R, Westermark P, Li JP: Heparan sulfate/heparin promotes transthyretin fibrillization through selective binding to a basic motif in the protein. Proc Natl Acad Sci USA 2011, 108:5584–5589
33. Goedert M, Jakes R, Spillantini MG, Hasegawa M, Smith MJ, Crowther RA: Assembly of microtubule-associated protein tau into Alzheimer-like filaments induced by sulphated glycosaminoglycans. Nature 1996, 383:550–553
34. McLaurin J, Franklin T, Zhang X, Deng J, Fraser PE: Interactions of Alzheimer amyloid-beta peptides with glycosaminoglycans effects on fibril nucleation and growth. Eur J Biochem 1999, 266:1101–1110
35. Castillo GM, Lukito W, Wight TN, Snow AD: The sulfate moieties of glycosaminoglycans are critical for the enhancement of beta-amyloid protein fibril formation. J Neurochem 1999, 72:1681–1687
36. Valle-Delgado JJ, Alfonso-Prieto M, de Groot NS, Ventura S, Samitier J, Rovira C, Fernandez-Busquets X: Modulation of Abeta42 fibrillogenesis by glycosaminoglycan structure. FASEB J 2010, 24:4250–4261
37. Li JP, Galvis ML, Gong F, Zhang X, Zcharia E, Metzger S, Vlodavsky I, Kisilevsky R, Lindahl U: In vivo fragmentation of heparan sulfate by heparanase overexpression renders mice resistant to amyloid protein A amyloidosis. Proc Natl Acad Sci USA 2005, 102:6473–6477
38. Timmer NM, Schirris TJ, Bruinsma IB, Otte-Holler I, van Kuppevelt TH, de Waal RM, Verbeek MM: Aggregation and cytotoxic properties towards cultured cerebrovascular cells of Dutch-mutated Abeta40 (DAbeta(1–40)) are modulated by sulfate moieties of heparin. Neurosci Res 2010, 66:380–389
39. Meyer-Luehmann M, Coomaraswamy J, Bolmont T, Kaeser S, Schaefer C, Kilger E, Neuenschwander A, Abramowski D, Frey P, Jaton AL, Vigouret JM, Paganetti P, Walsh DM, Mathews PM, Ghiso J, Staufenbiel M, Walker LC, Jucker M: Exogenous induction of cerebral beta-amyloidogenesis is governed by agent and host. Science 2006, 313:1781–1784
40. Timmer NM, Herbert MK, Kleinovink JW, Kiliaan AJ, De Waal RM, Verbeek MM: Limited expression of heparan sulphate proteoglycans associated with Abeta deposits in the APPswe/PS1dE9 mouse model for Alzheimer's disease. Neuropathol Appl Neurobiol 2010, 36:478–486
41. van den Born J, Salmivirta K, Henttinen T, Ostman N, Ishimaru T, Miyaura S, Yoshida K, Salmivirta M: Novel heparan sulfate structures revealed by monoclonal antibodies. J Biol Chem 2005, 280:20516–20523
42. Skovronsky DM, Lee VM, Trojanowski JQ: Neurodegenerative diseases: new concepts of pathogenesis and their therapeutic implications. Annu Rev Pathol 2006, 1:151–170
43. Kuret J, Chirita CN, Congdon EE, Kannanayakal T, Li G, Necula M, Yin H, Zhong Q: Pathways of tau fibrillization. Biochim Biophys Acta 2005, 1739:167–178
44. Perez M, Valpuesta JM, Medina M, Montejo de Garcini E, Avila J: Polymerization of tau into filaments in the presence of heparin: the minimal sequence required for tau-tau interaction. J Neurochem 1996, 67:1183–1190
45. Zhu HL, Fernandez C, Fan JB, Shewmaker F, Chen J, Minton AP, Liang Y: Quantitative characterization of heparin binding to Tau protein: implication for inducer-mediated Tau filament formation. J Biol Chem 2010, 285:3592–3599
46. Van Gool D, David G, Lammens M, Baro F, Dom R: Heparan sulfate expression patterns in the amyloid deposits of patients with Alzheimer's and Lewy body type dementia. Dementia 1993, 4:308–314
47. Donahue JE, Berzin TM, Rafii MS, Glass DJ, Yancopoulos GD, Fallon JR, Stopa EG: Agrin in Alzheimer's disease: altered solubility and abnormal distribution within microvasculature and brain parenchyma, Proc Natl Acad Sci USA 1999, 96:6468–6472
48. Verbeek MM, Otte-Holler I, van den Born J, van den Heuvel LP, David G, Wesseling P, de Waal RM: Agrin is a major heparan sulfate proteoglycan accumulating in Alzheimer's disease brain. Am J Pathol 1999, 155:2115–2125
49. van Horssen J, Otte-Holler I, David G, Maat-Schieman ML, van den Heuvel LP, Wesseling P, de Waal RM, Verbeek MM: Heparan sulfate proteoglycan expression in cerebrovascular amyloid beta deposits in Alzheimer's disease and hereditary cerebral hemorrhage with amyloidosis (Dutch) brains. Acta Neuropathol 2001, 102:604–614
50. Cappai R, Cheng F, Ciccotosto GD, Needham BE, Masters CL, Multhaup G, Fransson LA, Mani K: The amyloid precursor protein (APP) of Alzheimer disease and its paralog. APLP2, modulate the Cu/Zn-Nitric Oxide-catalyzed degradation of glypican-1 heparan sulfate in vivo, J Biol Chem 2005, 280:13913–13920
51. Carlsson P, Presto J, Spillmann D, Lindahl U, Kjellen L: Heparin/heparan sulfate biosynthesis: processive formation of N-sulfated domains. J Biol Chem 2008, 283:20008–20014
52. Lindahl B, Eriksson L, Lindahl U: Structure of heparan sulphate from human brain, with special regard to Alzheimer's disease, Biochem J 1995, 306 (Pt 1):177–184
53. Bruinsma IB, te Riet L, Gevers T, ten Dam GB, van Kuppevelt TH, David G, Kusters B, de Waal RM, Verbeek MM: Sulfation of heparan sulfate associated with amyloid-beta plaques in patients with Alzheimer's disease. Acta Neuropathol 2010, 119:211–220
54. Bailey TL, Rivara CB, Rocher AB, Hof PR: The nature and effects of cortical microvascular pathology in aging and Alzheimer's disease. Neurol Res 2004, 26:573–578
55. Meyer EP, Ulmann-Schuler A, Staufenbiel M, Krucker T: Altered morphology and 3D architecture of brain vasculature in a mouse model for Alzheimer's disease, Proc Natl Acad Sci USA 2008, 105:3587–3592
56. Paris D, Ganey N, Banasiak M, Laporte V, Patel N, Mullan M, Murphy SF, Yee GT, Bachmeier C, Ganey C, Beaulieu-Abdelahad D, Mathura VS, Brem S: Impaired orthotopic glioma growth and vascularization in transgenic mouse models of Alzheimer's disease. J Neurosci 2010, 30:11251–11258
57. Kalaria RN, Cohen DL, Premkumar DR, Nag S, LaManna JC, Lust WD: Vascular endothelial growth factor in Alzheimer's disease and experimental cerebral ischemia. Brain Res Mol Brain Res 1998, 62:101–105
58. Tarkowski E, Issa R, Sjogren M, Wallin A, Blennow K, Tarkowski A, Kumar P: Increased intrathecal levels of the angiogenic factors VEGF and TGF-beta in Alzheimer's disease and vascular dementia. Neurobiol Aging 2002, 23:237–243
59. Siedlak SL, Cras P, Kawai M, Richey P, Perry G: Basic fibroblast growth factor binding is a marker for extracellular neurofibrillary tangles in Alzheimer disease. J Histochem Cytochem 1991, 39:899–904
60. Iozzo RV: Matrix proteoglycans: from molecular design to cellular function. Annu Rev Biochem 1998, 67:609–652
61. Morimoto-Tomita M, Uchimura K, Bistrup A, Lum DH, Egeblad M, Boudreau N, Werb Z, Rosen SD: Sulf-2, a proangiogenic heparan sulfate endosulfatase, is upregulated in breast cancer. Neoplasia 2005, 7:1001–1010
62. Ryu JK, Cho T, Choi HB, Wang YT, McLarnon JG: Microglial VEGF receptor response is an integral chemotactic component in Alzheimer's disease pathology. J Neurosci 2009, 29:3–13
63. Zlokovic BV: Neurovascular mechanisms of Alzheimer's neurodegeneration. Trends Neurosci 2005, 28:202–208

Supplemental Figure S1

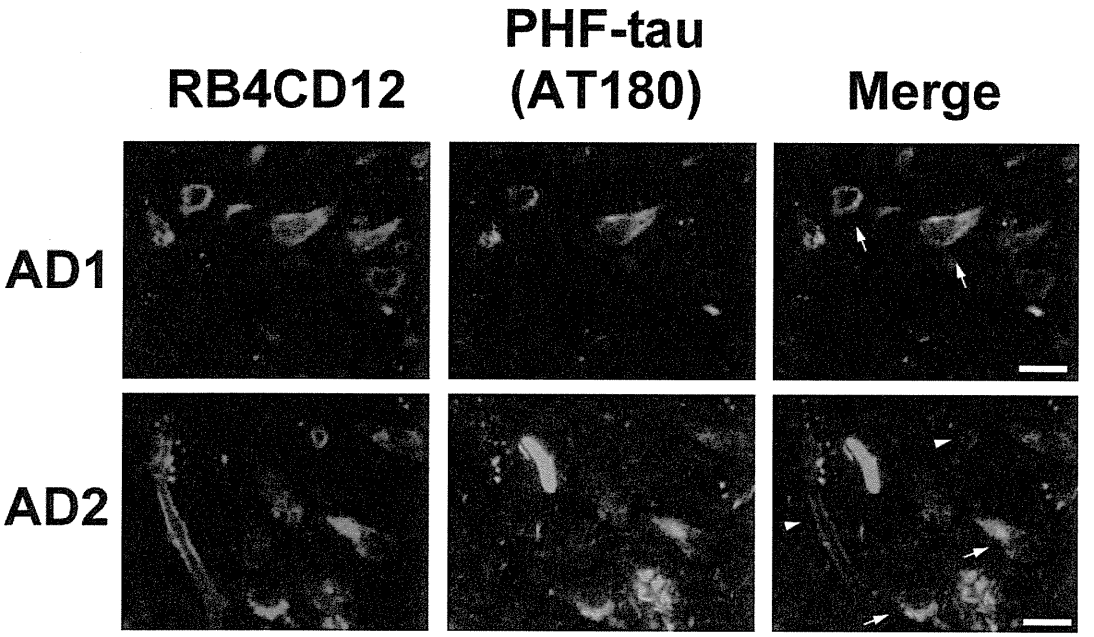

Immunohistochemistry for the RB4CD12 epitope and phosphorylated tau proteins. Postmortem brain sections of Alzheimer's disease (AD) patients (AD1, AD2) were subjected to heat-induced epitope retrieval and co-stained with RB4CD12 and biotinylated anti-paired helical filament (PHF)-tau antibody AT180 as described in Materials and Methods in the article. Primary antibodies were detected with Cy3-conjugated anti-VSV-G (red) and Cy2-conjugated streptavidin (green). Digital images were captured by fluorescent microscopy. Intracellular RB4CD12-staining signals were seen in some AT180-positive hippocampal neurons (arrows). Vessel-staining signals with RB4CD12 were observed (arrowheads). Bars: 25 μm.

Supplemental Figure S2

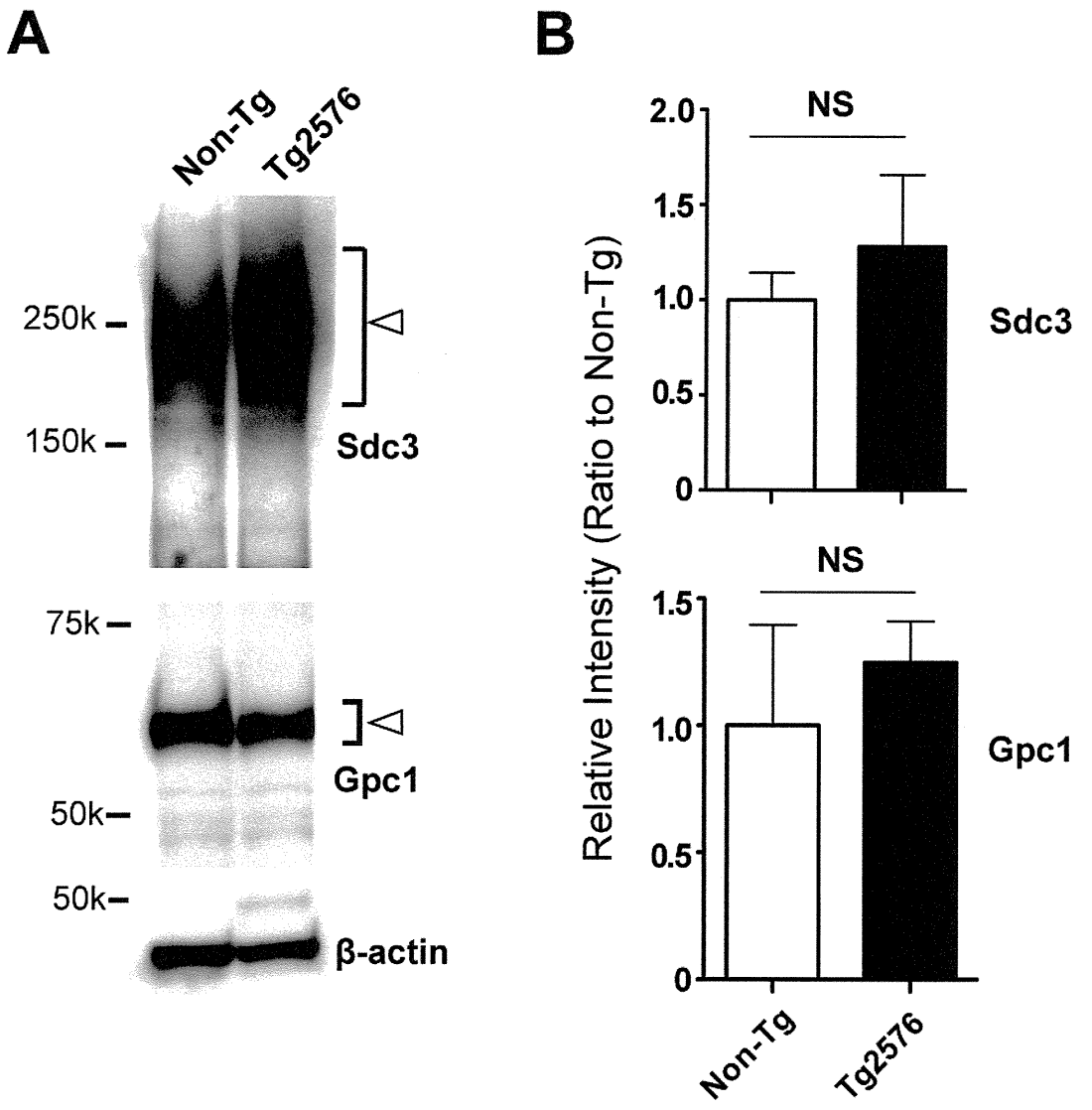

Immunoblotting analysis of syndecan-3 and glypican-1. A: Tris-buffered saline (TBS)-soluble and TBS-insoluble/1% SDS-soluble fractions were prepared from tissue homogenates of 20-month-old Tg2576 and age-matched non-Tg cortices. Immunoblots with anti-syndecan-3 antibody for TBS-insoluble/1% SDS-soluble fractions (Sdc3) and with anti-glypican-1 antibody for TBS-soluble fractions (Gpc1) were performed as described in Materials and Methods in the article. B: Relative intensities of bands indicated by open arrowheads in (A) were measured. N = 4, Tg2576; N = 5, Non-Tg; NS, not significant.

Journal of Histochemistry & Cytochemistry 60(5) 397–407

DOI: 10.1369/0022155412437613
http://jhc.sagepub.com
SAGE

Expression of Long-form *N*-Acetylglucosamine-6-*O*-Sulfotransferase 1 in Human High Endothelial Venules

Maiko Fujiwara, Motohiro Kobayashi, Hitomi Hoshino, Kenji Uchimura, Tsutomu Nakada, Junya Masumoto, Yasuhiro Sakai, Minoru Fukuda, and Jun Nakayama

Department of Molecular Pathology, Shinshu University Graduate School of Medicine, Matsumoto, Japan (MFujiwara,MK,JM,YS,JN); Department of Alzheimer's Disease Research, National Institute for Longevity Sciences, Obu, Japan (HH,KU); Department of Molecular Pharmacology, Shinshu University School of Medicine, Matsumoto, Japan (TN); and Glycobiology Unit, Cancer Research Center, Sanford-Burnham Medical Research Institute, La Jolla, California (MFukuda)

Summary

Two members of the *N*-acetylglucosamine-6-*O*-sulfotransferase (GlcNAc6ST) family, GlcNAc6ST-1 and GlcNAc6ST-2, function in the biosynthesis of 6-sulfo sialyl Lewis X–capped glycoproteins expressed on high endothelial venules (HEVs) in secondary lymphoid organs. Thus, both enzymes play a critical role in L-selectin-expressing lymphocyte homing. Human GlcNAc6ST-1 is encoded by a 1593-bp open reading frame exhibiting two 5′ in-frame methionine codons spaced 141 bp apart. Both resemble the consensus sequence for translation initiation. Thus, it has been hypothesized that both long and short forms of GlcNAc6ST-1 may be present, although endogenous expression of either form has not been confirmed in humans. Here, the authors developed an antibody recognizing amino acid residues between the first two human GlcNAc6ST-1 methionines. This antibody specifically recognizes the long form of the enzyme, a finding validated by Western blot analysis and immunofluorescence cytochemistry of HeLa cells misexpressing long and/or short forms of human GlcNAc6ST-1. Using this antibody, the authors carried out immunofluorescence histochemistry of human lymph node tissue sections and found endogenous expression of the long form of the enzyme in human tissue, predominantly in the *trans*-Golgi network of endothelial cells that form HEVs. (J Histochem Cytochem 60:397–407, 2012)

Keywords

N-acetylglucosamine-6-*O*-sulfotransferase 1 (GlcNAc6ST-1), long form, high endothelial venule (HEV)

Circulating lymphocytes routinely home to secondary lymphoid organs such as lymph nodes, tonsils, and Peyer's patches, where they recognize cognate antigens by interacting with antigen-presenting cells. Such homing is tightly regulated by sequential adhesive interactions. The initial step of the interaction, called "tethering and rolling," is mediated by the carbohydrate-binding protein L-selectin expressed on lymphocytes and by its carbohydrate ligand peripheral lymph node addressin (PNAd), expressed on the luminal surface of high endothelial venules (HEVs). This step is a prerequisite for subsequent lymphocyte chemokine-dependent activation, integrin-mediated firm attachment to the endothelium, and transmigration across blood vessels (Springer 1994; Butcher and Picker 1996; von Andrian and Mempel 2003). PNAd is expressed not only on HEVs in secondary lymphoid organs but also on HEV-like vessels induced in various non-lymphoid organs under chronic inflammatory states (Michie et al. 1993; Salmi et al. 1994; Renkonen et al. 2002; Kobayashi et al. 2004; Aloisi and Pujol-Borrell 2006). Moreover, PNAd is also expressed in gastric mucosa-associated lymphoid tissue (MALT) lymphoma, a neoplastic lesion resulting from chronic

Received for publication October 28, 2011; accepted January 9, 2012.

Corresponding Author:
Motohiro Kobayashi, Department of Molecular Pathology, Shinshu University Graduate School of Medicine, 3-1-1 Asahi, Matsumoto, Nagano 390-8621, Japan.
E-mail: motokoba@shinshu-u.ac.jp

Helicobacter pylori gastritis (Dogan et al. 1997; Kobayashi et al. 2011).

PNAd consists of a group of glycoproteins recognized by the MECA-79 monoclonal antibody (Streeter et al. 1988; Rosen 2004), which has an epitope that has been shown to be 6-sulfo *N*-acetyllactosamine (LacNAc) attached to extended core 1 *O*-glycans, Galβ1→4(sulfo→6)GlcNAcβ1 →3Galβ1→3GalNAcα1→Ser/Thr (Yeh et al. 2001). MECA-79 also recognizes the epitope's sialylated and fucosylated form, 6-sulfo sialyl Lewis X, attached to extended core 1 *O*-glycans, sialic acid2→3Galβ1→4[Fuc α1→3(sulfo→6)]GlcNAcβ1→3Galβ1→3GalNAcα1→ Ser/Thr. *N*-acetylglucosamine (GlcNAc)-6-*O*-sulfation of the sialyl Lewis X tetrasaccharide, which is critical for L-selectin binding (Imai et al. 1993), is catalyzed by GlcNAc-6-*O*-sulfotransferases (GlcNAc6STs), which transfer sulfate from 3′-phosphoadenosine 5′-phosphosulfate (PAPS) to the 6-*O* position of GlcNAc residues (Fukuda et al. 2001; Grunwell and Bertozzi 2002). Thus far, five members of the GlcNAc6ST family have been cloned in humans, four of which have murine orthologues (Uchimura and Rosen 2006). Among them, GlcNAc6ST-1 (Uchimura et al. 1998; Li and Tedder 1999) and GlcNAc6ST-2 (Bistrup et al. 1999; Hiraoka et al. 1999) have been confirmed to be expressed in HEVs, and both play a critical role in L-selectin ligand biosynthesis (Kawashima et al. 2005; Uchimura et al. 2005). Relevant to human pathological states, we previously reported that the number of PNAd-expressing HEV-like vessels in the colonic lamina propria is increased in active ulcerative colitis (UC) compared with the number seen in remission phase UC and that such an increase is associated with increased levels of transcripts encoding GlcNAc6ST-1 (Suzawa et al. 2007; Kobayashi et al. 2009).

GlcNAc6ST-1 is a type II transmembrane protein composed of a short N-terminal cytoplasmic tail, a hydrophobic single-pass transmembrane domain, an intervening stem region, and a C-terminal catalytic domain that resides in the Golgi lumen (Grunwell and Bertozzi 2002). Human GlcNAc6ST-1 was cloned as a 1593-bp open reading frame showing two in-frame methionine codons at the 5′ end, spaced 141 bp apart from each other. Both potential start sites agreed with the consensus sequence for translation initiation (Kozak 1991) (Fig. 1). One of the authors of this study previously proposed that both long and short forms of GlcNAc6ST-1 are expressed (Uchimura et al. 1998). Thus far, in vitro studies employing cell culture and misexpression of human GlcNAc6ST-1 have characterized the biochemistry and function of the enzyme in detail (Uchimura et al. 1998, 2002; Tangemann et al. 1999; Bhakta et al. 2000; Li et al. 2001; Grunwell et al. 2002; Lee et al. 2003; de Graffenried and Bertozzi 2003, 2004; Desko et al. 2009); however, most have used expression vectors harboring cDNA encoding short and/or even shorter engineered soluble forms of the enzyme. In the only study using an expression vector harboring the long-form cDNA, the authors confirmed its mRNA expression by Northern blot analysis; however, expression of the protein was not evaluated (Li et al. 2001). More important, expression of native human GlcNAc6ST-1 protein, regardless of form, has not yet been confirmed.

Figure 1. Nucleotide and deduced amino acid sequences of the N-terminal region of human GlcNAc6ST-1 (long form). The first two methionines are boxed, and the sequence encoding the putative transmembrane domain is doubly underlined. The sequence of the antigenic peptide used to produce anti-GlcNAc6ST-1-N antibody is underlined in bold.

In the present study, we developed an antibody recognizing amino acid residues between the first two methionines (designated M#1 and M#2, respectively) of human GlcNAc6ST-1 and found that the long form of the enzyme is endogenously expressed in humans, predominantly in the *trans*-Golgi network (TGN) of endothelial cells that form HEVs. We also found that both forms of the enzyme show comparable subcellular localization and intracellular enzymatic activity.

Materials and Methods

Generation of an Antibody against the N-Terminal Site of Human Long-Form GlcNAc6ST-1

We generated a polyclonal antibody recognizing only the long form of human GlcNAc6ST-1 by directing it to residues between M#1 and M#2. An immunogenic peptide, NH_2-C+LPQWPRRPGRRWPA-COOH, corresponding to amino acids 30 to 43 of human GlcNAc6ST-1 (Fig. 1, bold line), was chemically synthesized and conjugated with keyhole limpet hemocyanin (KLH). The KLH-conjugated peptide was mixed with Freund's complete adjuvant and subcutaneously injected into a Japanese white rabbit, followed by four additional injections with Freund's incomplete adjuvant at 2-week intervals. The antibody was purified by affinity chromatography on a column coupled to the immunogenic peptide. The purified antibody, designated anti-GlcNAc6ST-1-N,

was used for subsequent experiments. The experimental protocol was approved by the Institutional Animal Care and Use Committee at Operon Biotechnologies (Tokyo, Japan).

Construction of Expression Vectors Encoding Long and Short Forms of Human GlcNAc6ST-1 with or without a FLAG Tag

pcDNA1-GlcNAc6ST-1 M#1 encoding the long form of human GlcNAc6ST-1 was constructed previously (Kobayashi et al. 2009). pcDNA1-GlcNAc6ST-1 M#1-FLAG, which encodes the long form with a FLAG epitope tag fused to its C-terminus, was similarly constructed using the polymerase chain reaction (PCR) by replacing the 3′-primer with 5′-AATCTAGATTA**TTTGTCGTCGTC ATCCTTATAATC**CTCGAGGAGACGGGGCTTC CGAAGCAG-3′ (*Xba*I site underlined; FLAG epitope tag bolded). Similarly, pcDNA1-GlcNAc6ST-1 M#2 encoding the short form of GlcNAc6ST-1 and pcDNA1-GlcNAc6ST-1 M#2-FLAG were constructed by replacing the 5′-primer with 5′-TCGAATTCCCCTCTCGGAATGAAGGTGTT-3′ (*Eco*RI site underlined). All constructs established here have an identical sequence outside the insert.

Expression of Human GlcNAc6ST-1 in HeLa Cells

HeLa cells were transiently transfected with one of the above expression vectors using Lipofectamine Plus (Invitrogen; Carlsbad, CA), according to the manufacturer's instructions, and analyzed 24 to 48 hr after transfection. To express long and short forms of GlcNAc6ST-1 simultaneously, HeLa cells were cotransfected with pcDNA1-GlcNAc6ST-1 M#1 and pcDNA1-GlcNAc6ST-1 M#2-FLAG at a ratio of 1:1.

Western Blot Analysis

HeLa cell transfectants were harvested in phosphate-buffered saline (PBS) supplemented with Complete Mini protease inhibitor (Roche; Basel, Switzerland) with a cell scraper and subjected to three cycles of freeze/thawing to disrupt the plasma membrane. The membrane fraction was collected by centrifugation at 12,000 × *g* for 10 min and resuspended in 10 mM Tris/HCl and 1 mM EDTA (pH 8.0). Subsequently, 10% Triton X-100 was added to a final concentration of 1%, the mixture was gently rocked at 4C for 15 min, and the Triton X-100-soluble membrane fraction was obtained by centrifugation at 12,000 × *g* for 10 min. To remove *N*-glycans on the protein, an aliquot of each membrane fraction containing 5 μg protein was treated with 125 units of peptide *N*-glycosidase F (PNGase F) (New England Biolabs; Ipswich, MA) at 37C for 2 hr, lysed in sample buffer, and incubated at 95C for 5 min. Each sample was separated by sodium dodecyl sulfate–polyacrylamide gel electrophoresis (SDS-PAGE) using SuperSep Ace 7.5% (Wako Pure Chemical Industries; Osaka, Japan) and transferred onto a polyvinylidene difluoride (PVDF) membrane (Millipore; Billerica, MA). After blocking with Tris-buffered saline (TBS) (pH 7.6) supplemented with 5% skim milk and 0.1% Tween-20 for 60 min, the membrane was incubated with anti-GlcNAc6ST-1-N (1:1000) and anti-FLAG M2 (Sigma-Aldrich; St. Louis, MO) (1:5000) at 4C overnight, followed by incubation with horseradish peroxidase (HRP)–conjugated anti-rabbit IgG (Cell Signaling Technology; Danvers, MA) (1:2500) and anti-mouse IgG (Immuno-Biological Laboratories; Gunma, Japan) (1:5000), respectively, for 60 min. Immunoreactive bands were visualized using SuperSignal West Dura Extended Duration Substrate (Thermo Scientific; Rockford, IL) and a luminescent image analyzer LAS-3000 (Fuji Film; Tokyo, Japan).

Immunofluorescence Staining

For immunofluorescence cytochemistry, HeLa cell transfectants grown on coverslips were fixed with 20% neutral-buffered formalin for 15 min, and cell membranes were permeabilized with 0.1% Triton X-100 in PBS for 15 min. For immunofluorescence histochemistry, fresh human lymph node tissues were embedded in Tissue-Tek OCT compound (Sakura Finetek; Tokyo, Japan) and frozen at −80C. Frozen tissues were sectioned at 6 μg, fixed with acetone for 5 min, and air-dried. Use of human lymph node tissues was approved by the Ethics Committee of Shinshu University School of Medicine. After blocking with 1% bovine serum albumin (BSA) (Sigma-Aldrich) in TBS for 15 min, samples were incubated with a cocktail of two primary antibodies for 15 min. After washing, samples were incubated for 15 min with a cocktail of two isotype-matched secondary antibodies differentially labeled with Alexa Fluor 488 and Alexa Fluor 555 (Invitrogen) (1:1000). Samples were mounted with Vectashield mounting medium (Vector Laboratories; Burlingame, CA) and observed under a fluorescence microscope AX-80 (Olympus; Tokyo, Japan). Primary antibodies used for immunofluorescence are listed in Table 1.

Cell Enzyme-Linked Immunosorbent Assay

HeLa cells were seeded into 96-well plates (BD Falcon; Franklin Lakes, NJ) at 2 × 10^4 cells/well and 24 hr later transiently transfected with one of the following expression vectors: pcDNA1-GlcNAc6ST-1 M#1, pcDNA1-GlcNAc6ST-1 M#2, pcDNA1-GlcNAc6ST-2, and pcDNA1 (mock). Forty-eight hours later, cells were fixed with 20% neutral-buffered formalin for 15 min. To quench endogenous peroxidase activity, cells were treated with

Table 1. Primary Antibodies Used for Immunofluorescence Staining

Name	Clone	Isotype	Source	Dilution
Anti-GlcNAc6ST-1-N	—	Rabbit polyclonal	This study	1:250
Anti-FLAG	M2	Mouse IgG_1	Sigma-Aldrich, St. Louis, MO	1:250
Anti-PNAd	MECA-79	Rat IgM	BD Pharmingen, San Diego, CA	1:100
Anti-GM130	35/GM130	Mouse IgG_1	BD Bioscience, San Jose, CA	1:25
Anti-GS27	25/GS27	Mouse IgG_1	BD Bioscience, San Jose, CA	1:100
Anti-Rab8	4/Rab4	Mouse IgG_{2b}	BD Bioscience, San Jose, CA	1:100

0.3% hydrogen peroxide in absolute methanol for 30 min and washed with TBS. After blocking with 1% BSA in TBS for 30 min, cells were incubated for 60 min with 0.5 μg/ml of S2 monoclonal antibody recognizing 6-sulfo sialyl LacNAc on *N*- and *O*-glycans (Hirakawa et al. 2010). After washing with TBS, cells were incubated with HRP-conjugated anti-mouse IgM (Jackson ImmunoResearch; West Grove, PA) (1:5000) for 60 min. After washing, 100 μl of 1-Step ABTS (Thermo Scientific) was applied to each well, and absorbance at 405 nm was read using a microplate reader (DS Pharma Biomedical; Osaka, Japan).

Fluorescence-Activated Cell Sorting Analysis

HeLa cell transfectants were dissociated into mono-dispersed cells in PBS containing 0.5 mM EDTA and fixed with 20% neutral-buffered formalin for 15 min. Cells were then permeabilized with PBS/0.1% Triton X-100 for 15 min and incubated with anti-FLAG M2 (1:250), followed by Alexa Fluor 488–conjugated anti-mouse IgG (1:1000). Stained cells were analyzed using FACSort (BD Biosciences; San Jose, CA) with FlowJo software (Tree Star; Ashland, OR).

Semi-Quantitative Reverse Transcriptase PCR

Semi-quantitative reverse transcriptase PCR (RT-PCR) was carried out essentially as described (Kobayashi 2006). Total RNA was extracted from HeLa cell transfectants using ISOGEN reagent (Nippon Gene; Tokyo, Japan) according to the manufacturer's instructions. Single-stranded cDNA was synthesized as described (Suzawa et al. 2007). PCR was then carried out with primers for GlcNAc6ST-1, 5′-TCCTCCAAGCCTTTCGTGGTATCT-3′ (5′-primer) and 5′-TGGTAGCAAAACTCCTCCACCTGT-3′ (3′-primer), and glyceraldehyde-3-phosphate dehydrogenase (GAPDH), 5′-TGAGTACGTCGTGGAGTCCACT-3′ (5′-primer) and 5′-CAGAGATGATGACCCTTTTGGCTC-3′ (3′-primer). After initial denaturation at 94C for 2 min, 24 cycles of amplification with denaturation at 96C for 20 sec, annealing at 65C for 30 sec, and extension at 72C for 30 sec were performed, followed by a final extension at 72C for 2 min. PCR products were electrophoresed on 2% agarose gels containing 0.1 μg/ml ethidium bromide.

Statistical Analysis

Data are expressed as means ± SD. Differences among groups were statistically analyzed by one-way analysis of variance (ANOVA) with Bonferroni's posttest, using InStat 3 software (GraphPad Software; San Diego, CA). p values less than 0.05 were considered significant.

Results

Anti-GlcNAc6ST-1-N Specifically Recognizes the Long Form of GlcNAc6ST-1

To determine whether anti-GlcNAc6ST-1-N selectively recognizes the long form of GlcNAc6ST-1, the membrane fraction of HeLa cell transfectants was subjected to Western blot analysis. As shown in Fig. 2 (left panel), immunoblotting with anti-FLAG of samples not treated with PNGase F showed multiple immunoreactive bands migrating at ~60 kDa for the long form and ~55 kDa for the short form. In addition, immunoreactive species migrating at >100 kDa, the molecular weight of enzyme homodimers, were also detected with both forms of the enzyme, as described previously (de Graffenried and Bertozzi 2004). The appearance of multiple bands is consistent with a previous study using HeLa cells transfected with wild-type or mutant forms of GlcNAc6ST-1, which demonstrated that at least three of four potential *N*-glycosylation sites were glycosylated (Desko et al. 2009). Indeed, PNGase F digestion converted the multiple bands into a single major band migrating at ~55 kDa for the long form and ~50 kDa for the short form. By contrast, immunoblots using anti-GlcNAc6ST-1-N (Fig. 2, right panel) revealed immunoreactive species only for the long form, and the migration patterns of these bands were similar to those detected by immunoblotting with anti-FLAG.

We then performed double immunofluorescence staining of HeLa cell transfectants using anti-FLAG and anti-GlcNAc6ST-1-N antibodies. Cells transfected with pcDNA1-GlcNAc6ST-1 M#1-FLAG and pcDNA1-GlcNAc6ST-1 M#2-FLAG exhibited FLAG signals chiefly in a perinuclear, punctate pattern (Fig. 3, left panels). By contrast, anti-GlcNAc6ST-1-N antibody stained only cells transfected with pcDNA1-GlcNAc6ST-1 M#1-FLAG and pcDNA1-GlcNAc6ST-1 M#1, that is, expression vectors

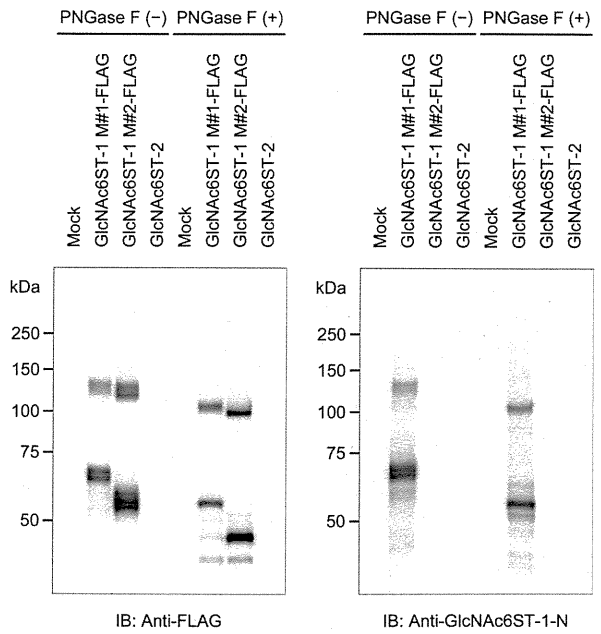

Figure 2. Western blot analysis of long and short forms of human GlcNAc6ST-1. The membrane fraction of HeLa cells transiently transfected with pcDNA1 (mock), pcDNA1-GlcNAc6ST-1 M#1-FLAG, pcDNA1-GlcNAc6ST-1 M#2-FLAG, or pcDNA1-GlcNAc6ST-2, with or without PNGase F digestion, was subjected to sodium dodecyl sulfate–polyacrylamide gel electrophoresis and probed with anti-FLAG (left panel) and anti-GlcNAc6ST-1-N (right panel) antibodies. Molecular weights are indicated to the left of each blot.

harboring cDNA encoding the long form of GlcNAc6ST-1 (Fig. 3, middle panels). In the case of cells transfected with pcDNA1-GlcNAc6ST-1 M#1-FLAG (Fig. 3, second row), the staining pattern of anti-GlcNAc6ST-1-N was similar to that of anti-FLAG, as judged by yellow signals seen in the merged image (Fig. 3, right panels). Overall, these findings indicate that the anti-GlcNAc6ST-1-N antibody specifically recognizes the GlcNAc6ST-1 long form.

Comparable Subcellular Localization of the Long and Short Forms of GlcNAc6ST-1

To determine potential differences in subcellular localization of long and short GlcNAc6ST-1 forms, HeLa cells cotransfected with pcDNA1-GlcNAc6ST-1 M#1 and pcDNA1-GlcNAc6ST-1 M#2-FLAG were subjected to double immunofluorescence staining with anti-GlcNAc6ST-1-N (for the long form) and anti-FLAG (for the short form) (Fig. 4A). As shown in Fig. 4B, signals for the long form showed a perinuclear punctate pattern, indicative of the Golgi apparatus, and almost all signals colocalized with those for the short form, indicating that the subcellular localization of both forms does not differ substantially.

Long and Short Forms of Human GlcNAc6ST-1 Show Comparable Intracellular GlcNAc-6-O-Sulfation Activity

To evaluate potential differences in intracellular GlcNAc-6-*O*-sulfation activity between long and short GlcNAc6ST-1 forms, cell enzyme-linked immunosorbent assays (ELISAs) for sulfation activity were carried out using HeLa cell transfectants. As shown in Fig. 5A, all GlcNAc6ST transfectants tested showed intracellular GlcNAc-6-*O*-sulfation activity, as assessed by reactivity of the S2 monoclonal antibody, which recognizes 6-sulfo sialyl LacNAc on *N*- and *O*-glycans (Hirakawa et al. 2010). The activity difference between both forms of GlcNAc6ST-1 was not statistically significant, but both GlcNAc6ST-1 forms demonstrated higher intracellular GlcNAc-6-*O*-sulfation activities than did GlcNAc6ST-2 ($p<0.05$).

We next performed fluorescence-activated cell sorting (FACS) analysis of HeLa cell transfectants to evaluate expression levels of long and short forms of GlcNAc6ST-1 protein. As shown in Fig. 5B, expression of the short-form protein (right panel) was higher compared with that of the long form (left panel). This finding confirms findings from our Western blot analysis that demonstrated that the intensity of immunoreactive bands representing the short form of the protein was greater than that of the long form (Fig. 2, left panel). In addition, semi-quantitative RT-PCR demonstrated that mRNA expression of short-form GlcNAc6ST-1 was higher than that of the long form (Fig. 5C).

The Long Form of GlcNAc6ST-1 Is Expressed Endogenously in Human HEVs

Finally, to determine whether the GlcNAc6ST-1 long form is endogenously expressed in human tissues, we performed double immunofluorescence staining of human lymph node tissue sections using anti-GlcNAc6ST-1-N and the anti-PNAd antibody MECA-79. As shown in Fig. 6A, MECA-79 clearly stained HEVs, predominantly the cell membrane of endothelial cells. By contrast, anti-GlcNAc6ST-1-N signals were detected in HEVs in a cytoplasmic perinuclear punctate pattern, indicative of the Golgi apparatus. This anti-GlcNAc6ST-1-N staining was abolished by addition of the peptide used for immunization (Fig. 6B), confirming antibody specificity.

To determine the sub-Golgi localization of this staining, we undertook double immunofluorescence staining for anti-GlcNAc6ST-1-N and a battery of Golgi markers. As shown in Fig. 6C, anti-GlcNAc6ST-1-N signals colocalized with those of Rab8, a membrane marker of the TGN (Chen et al. 1993), and partially colocalized with the *medial*-to-*trans*-Golgi marker GS27 (Lowe et al. 1997). Anti-GlcNAc6ST-1-N signals did not colocalize with the *cis*-Golgi marker GM130 (Nakamura et al. 1995). These findings, taken

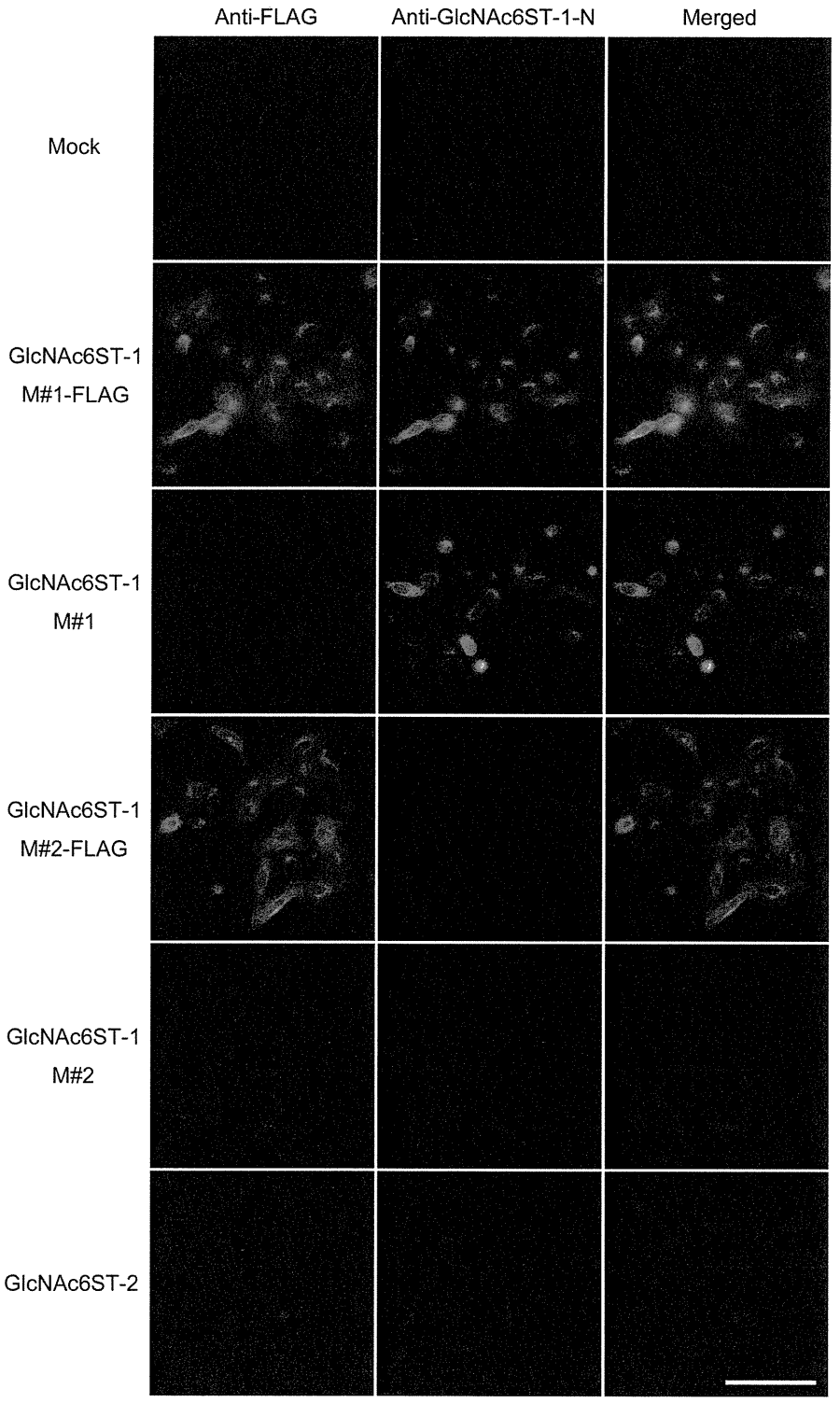

Figure 3. Specificity of anti-GlcNAc6ST-1-N antibody as assessed by immunofluorescence cytochemistry. HeLa cells were transiently transfected with expression vectors harboring cDNA encoding long (M#1) and short (M#2) forms of human GlcNAc6ST-1 with or without a FLAG epitope tag, as well as GlcNAc6ST-2 and mock (pcDNA1) as controls. Cells were doubly immunostained with anti-FLAG (green) and anti-GlcNAc6ST-1-N (red). Yellow signals in merged images indicate colocalization of the two antigens. Bar = 100 μm.

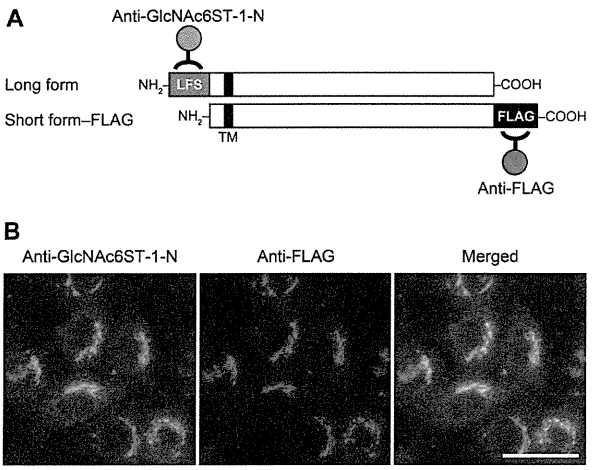

Figure 4. Subcellular localization of long and short forms of human GlcNAc6ST-1. (A) Schematic representation of long-form GlcNAc6ST-1 and short-form GlcNAc6ST-1 with a FLAG epitope tag. The antibody-binding site for anti-GlcNAc6ST-1-N (green) and anti-FLAG (red) is also indicated. LFS, long form–specific site. (B) HeLa cells doubly transfected with pcDNA1-GlcNAc6ST-1 M#1 and pcDNA1-GlcNAc6ST-1 M#2-FLAG were subjected to dual immunofluorescence staining for anti-GlcNAc6ST-1-N (green) and anti-FLAG (red). Yellow signals in merged images indicate colocalization of the two antigens. Bar = 50 μm.

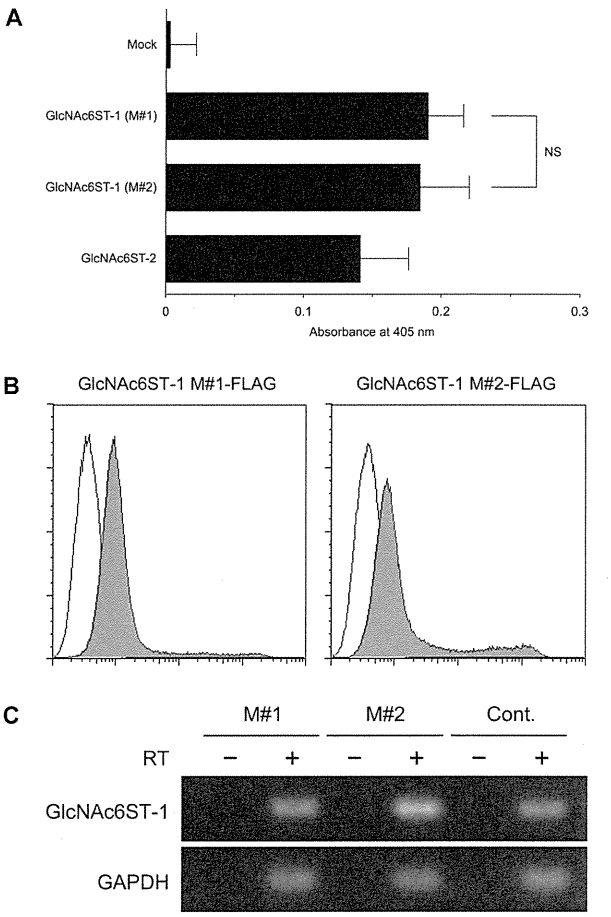

Figure 5. (A) Cell enzyme-linked immunosorbent assay (ELISA) showing intracellular GlcNAc-6-*O*-sulfation activity of GlcNAc6ST-1 M#1 and GlcNAc6ST-1 M#2. HeLa cells were transiently transfected with pcDNA1-GlcNAc6ST-1 M#1 and pcDNA1-GlcNAc6ST-1 M#2, as well as pcDNA1-GlcNAc6ST-2 and pcDNA1 (mock) as controls, and subjected to cell ELISA for S2 monoclonal antibody recognizing 6-sulfo sialyl LacNAc on *N*- and *O*-glycans. Data are expressed as means ± SD (n = 8 for each group). NS, not significant. (B) Intracellular expression levels of long (left panel) and short (right panel) forms of GlcNAc6ST-1 protein with a C-terminal FLAG epitope tag (gray histograms). Cells were stained for FLAG and subjected to fluorescence-activated cell sorting analysis. Open histograms represent negative control resulting from omitting the primary antibody. The x- and y-axes indicate fluorescence intensity and number of events, respectively. (C) Semi-quantitative RT-PCR showing mRNA expression levels of HeLa cells transfected with long (M#1) and short (M#2) forms of GlcNAc6ST-1 cDNA. Each RNA sample was treated with (+) or without (–) reverse transcriptase (RT). Cont., control amplification using distilled water (–) and plasmid harboring the target cDNA (+). GAPDH, glyceraldehyde-3-phosphate dehydrogenase.

together, indicate that the long form of GlcNAc6ST-1 is endogenously expressed in human endothelial cells of HEVs and localizes primarily to the TGN.

Discussion

In the present study, we developed an antibody specific for the long form of human GlcNAc6ST-1. Previously, one of the authors of this article reported that human GlcNAc6ST-1 cDNA potentially encodes long and short isoforms (Uchimura et al. 1998). However, most in vitro studies of human GlcNAc6ST-1 have employed expression vectors encoding the short and/or soluble forms of the enzyme, which lack a putative 47–amino acid N-terminal cytoplasmic tail. Moreover, expression of native human GlcNAc6ST-1 protein has not been confirmed. This prompted us to clarify whether the long form of the enzyme is endogenously expressed in humans. Employing the antibody developed here, we found that the long form of GlcNAc6ST-1 protein is endogenously expressed in human tissues, predominantly in endothelial cells that form HEVs.

Western blot analysis indicated that both forms of GlcNAc6ST-1 protein migrate as multiple bands of different molecular weights, consistent with previous reports (de Graffenried and Bertozzi 2003, 2004; Desko et al. 2009). Similar to other Golgi-resident proteins, GlcNAc6ST-1 displays four consensus sequences for *N*-glycosylation (Bause 1983). Desko et al. (2009) determined that three of those are indeed modified with *N*-glycans—namely, N196, N410, and N428 (N243, N457, and N475 for the long form).

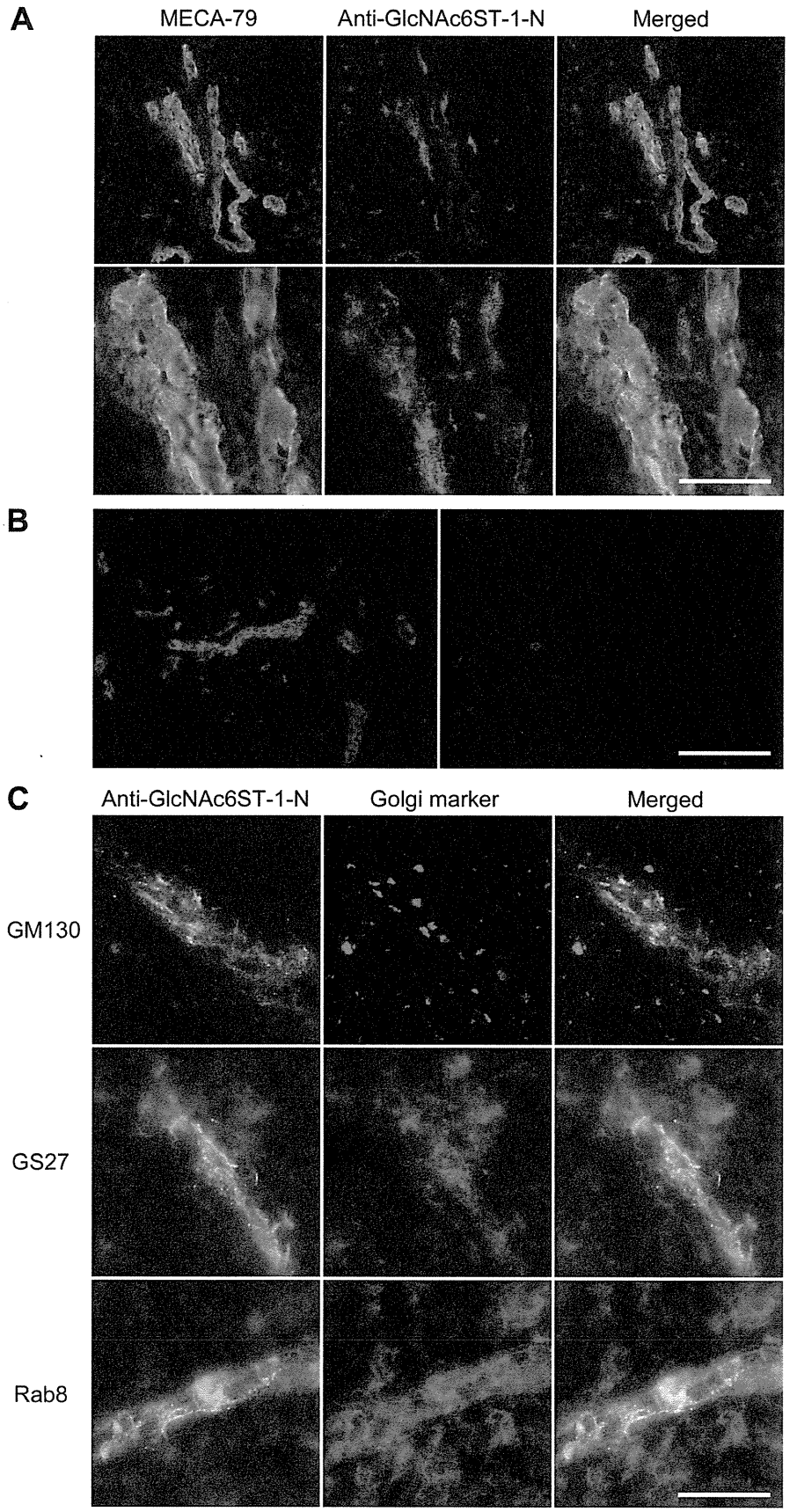

Figure 6. Endogenous expression of long-form GlcNAc6ST-1 protein as revealed by immunofluorescence histochemistry of human lymph node tissue sections. (A) Double immunofluorescence staining with MECA-79 (green) and anti-GlcN Ac6ST-1-N (red). Lower panels are enlarged images of the upper panels. Bar = 100 μm for upper panels and 25 μm for lower panels. (B) A competitive inhibition assay on tissue sections for anti-GlcNAc6ST-1-N binding in which antibody is preincubated at 4C overnight with 5 μg/ml of synthetic peptide used for immunization. Anti-GlcNAc6ST-1 staining on high endothelial venules (left panel) was abolished by this procedure (right panel). Bar = 100 μm. (C) Double immunofluorescence staining with anti-GlcNAc6ST-1-N (green) and one of the following Golgi markers (red): *cis*-Golgi marker GM130 (upper panels), *medial*-to-*trans*-Golgi marker GS27 (middle panels), and a *trans*-Golgi network marker to plasma membrane protein Rab8 (lower panels). Bar = 25 μm.

Consistently, pretreatment with PNGase F altered the size of immunoreactive species of both long and short forms of GlcNAc6ST-1 expressed in HeLa cells.

We also employed HeLa cell transfectants to compare subcellular localization and intracellular enzymatic activity of both forms. Double immunofluorescence staining of HeLa cells transfected with both GlcNAc6ST-1 forms revealed no gross difference in their subcellular localization. It is noteworthy that β1,4-galactosyltransferase 1 (β4GalT-1), a type II membrane-bound enzyme that transfers galactose (Gal) to acceptor sugars in a β1,4-linkage, also exists in long and short forms (Lopez et al. 1991). Both forms share an 11–amino acid cytoplasmic tail, but the long form exhibits an additional 13–amino acid sequence and is preferentially targeted to the plasma membrane, whereas the short form resides primarily within the Golgi compartment. In addition to β4GalT-1, differential subcellular localization of two enzyme isoforms has been recently reported for glucuronyltransferase P (GlcAT-P) and lactosylceramide α2,3-sialyltransferase (GM3 synthase) (Kizuka et al. 2009; Uemura et al. 2009). However, our study shows that, unlike these enzymes, the 47–amino acid sequence in the short cytoplasmic tail of long-form GlcNAc6ST-1 does not affect its subcellular localization.

Cell ELISAs carried out in the present study also showed that both long and short forms of GlcNAc6ST-1 demonstrate comparable intracellular GlcNAc-6-*O*-sulfation activity. Catalytic properties and substrate specificities of N-terminally truncated/protein A fusions of human GlcNAc6STs were previously reported (Uchimura et al. 2002). In that study, both N-terminally truncated, soluble GlcNAc6ST-1 and the full-length short form of transmembrane GlcNAc6ST-1 showed similar substrate specificities and enzymatic activity, which is consistent with the present finding. It should be noted that expression of the short-form GlcNAc6ST-1 protein exceeded that of the long form, as evaluated by FACS and Western blot analyses. It is possible that long-form GlcNAc6ST-1 may exhibit higher GlcNAc-6-*O*-sulfation activity. Alternatively, the short form might have difficulty accessing the substrate, leading to less product elaboration. Considering the results of semi-quantitative RT-PCR analysis, the higher expression of the short-form GlcNAc6ST-1 protein is likely due to higher mRNA expression level compared with that seen for the long form.

Among GlcNAc6ST family members, GlcNAc6ST-1 is unique in having an N-terminal long cytoplasmic tail (in the long form) and an intervening stem region between the transmembrane and catalytic domains. A previous study reported that GlcNAc6ST-1 sulfotransferase is confined to the TGN, whereas GlcNAc6ST-2 is distributed throughout the Golgi apparatus (de Graffenried and Bertozzi 2003). To clarify the mechanism underlying differential localization, those authors constructed a chimera comprising the localization domain (for the short form) and the stem region of GlcNAc6ST-1 fused to the GlcNAc6ST-2 catalytic domain and found that the chimeric protein was confined to the TGN and adopted GlcNAc6ST-1 substrate preference. Our result is consistent with these results because both long and short forms of GlcNAc6ST-1 expressed in HeLa cells contain the putative localization domain proposed by these authors.

Although short-form GlcNAc6ST-1 can be misexpressed in HeLa cells in vitro, it is not known whether the short form is indeed expressed endogenously in humans. It has been reported that a suboptimal context around the first AUG codon causes some 40S ribosomal subunits to bypass the first AUG and initiate at a second AUG codon (Kozak 1989, 1991). Given our observation of endogenous long-form GlcNAc6ST-1, future studies are required to determine whether the short form is also expressed in vivo.

Acknowledgments

The authors thank Drs. Tomoya Akama and Nagako Kawashima for useful discussion, Dr. Hiroto Kawashima for providing S2 monoclonal antibody, Mses. Kayo Suzuki and Yasuyo Shimojo for technical assistance, and Dr. Elise Lamar for critical reading of the manuscript. Part of the work was presented as a poster at the Annual Meeting of the Society for Glycobiology, held in Seattle, Washington, November 9–12, 2011.

Declaration of Conflicting Interests

The authors declared no potential conflicts of interest with respect to the research, authorship, and/or publication of this article.

Funding

The authors disclosed receipt of the following financial support for research and/or authorship of this article: This work was supported by Grant-in-Aid for Young Scientists 20790278, 22790343 (both to MK), 23790426 (to HH), and 22790303 to (KU) from the Ministry of Education, Culture, Sports, Science and Technology of Japan; Grant-in-Aid for Scientific Research 21390104 from the Japan Society for the Promotion of Science (to JN); and Grant PO1 CA71932 from the National Institutes of Health (to MFukuda).

References

Aloisi F, Pujol-Borrell R. 2006. Lymphoid neogenesis in chronic inflammatory diseases. Nat Rev Immunol. 6:205–217.

Bause E. 1983. Structural requirements of *N*-glycosylation of proteins: studies with proline peptides as conformational probes. Biochem J. 209:331–336.

Bhakta S, Bartes A, Bowman KG, Kao WM, Polsky I, Lee JK, Cook BN, Bruehl RE, Rosen SD, Bertozzi CR, et al. 2000. Sulfation of *N*-acetylglucosamine by chondroitin 6-sulfotransferase 2 (GST-5). J Biol Chem. 275:40226–40234.

Bistrup A, Bhakta S, Lee JK, Belov YY, Gunn MD, Zuo FR, Huang CC, Kannagi R, Rosen SD, Hemmerich S. 1999. Sulfotransferases of two specificities function in the reconstitution of high endothelial cell ligands for L-selectin. J Cell Biol. 145:899–910.